

## 4 Composite Filter Design

### 4.1 Introduction

Harmonic distortion in power distribution systems can be suppressed using two approaches namely, passive and active filtering. The passive filtering is the simplest conventional solution to mitigate the harmonic distortion [103] discussed in detail in chapter 3. Although simplest and least expensive, the use passive elements do not always respond correctly to the dynamics of the power distribution systems and hence it inherits several shortcomings [52]:

- The filter components are very bulky because the harmonics that need to be suppressed are usually of the low order.
- The compensation characteristics of these filters are influenced by the source impedance.
- The filter design is heavily dependent on the power system in which it is connected to.
- Passive filters are known to cause resonance, thus affecting the stability of the power distribution systems.
- Frequency variation of the power distribution system and tolerances in components values affect the filtering characteristics.
- The size of the components become impractical if the frequency variation is large
- As the regulatory requirements become more stringent, the passive filters might not be able to meet future revisions of a particular Standard. This may require a retrofit of new filters.

The hybrid/composite topologies aimed to enhance the passive filter performance and power rating reduction of the active filter. Two configurations have been mainly proposed: active filter connected in series with the shunt passive filter and series active filter combined with shunt passive filter. Both the topologies are useful to compensate current harmonics.

However, when the load also generates voltage harmonics, the second topology is most appropriate. Electric arc furnace is a typical case of voltage harmonic load along with current harmonics, that's why the topology used is series active filter combined with shunt passive filter. Combined operation of series APF with traditional passive filter i.e. composite filter is found one of the solutions to overcome the disadvantages of the existing passive filters. It controlled to act as a harmonic isolator between the source and nonlinear load by injection of a controlled harmonic voltage source [52]-[53], [104].

## 4.2 Basic Compensation Principle

As shown in Figure 4.1 a series APF, typically, consists of a three phase PWM inverter.

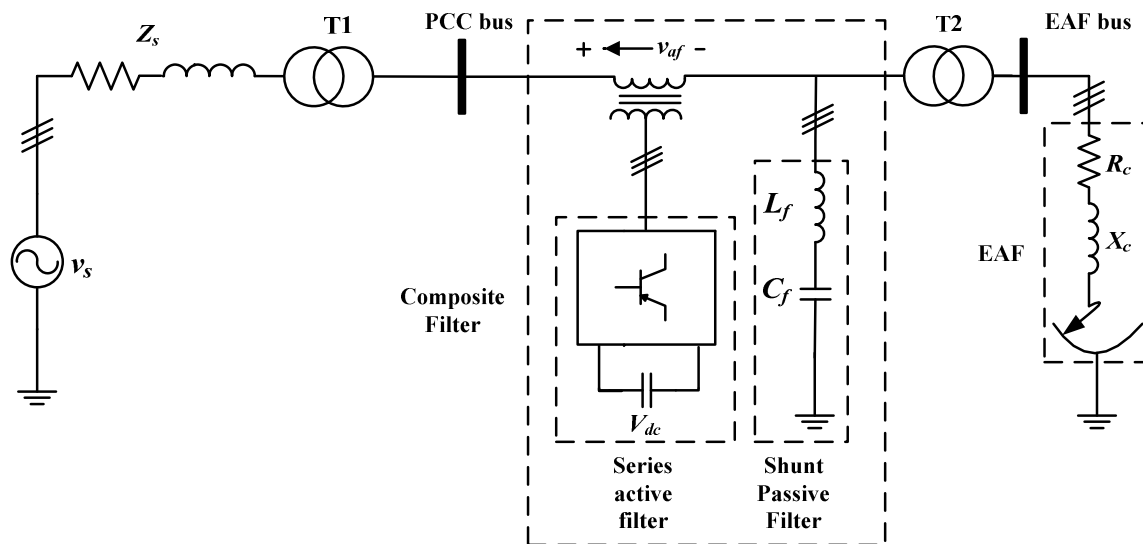


Figure 4.1 PQ improvement using CF

When this equipment is connected in series to the AC source impedance it is possible to improve the compensation characteristic of passive filter connected in parallel. This combined topology is known as composite filter shown in Figure 4.1, where the series active filter acts as controlled voltage source. Voltage  $v_{af}$  is the voltage that the said inverter should generate to improve the power quality.

### 4.3 Design of Reference Voltage and Control Scheme

During last decade, substantial research has been carried out in innovating different new configurations and in control techniques used for harmonic mitigation in power system. Various control strategies have been applied to obtain the control signals for the series active filter surveyed in the literature [9], [43]-[44], [53],[56], [60], [63], [66], [104]-[112].

B. Singh, K. Al-Haddad [9], he presents a comprehensive review of active filter configurations, control strategies, selection of components, other related economic and technical considerations, and their selection for specific applications.

F. Zheng Peng [42], he a combined system of shunt passive and small rated series filters has already been proposed by the authors. The operating principle and steady compensation characteristics have been presented as well.

Hideaki Fujita [43], he presents a combined system of a passive filter and a small-rated active filter, both connected in series with each other. The passive filter removes load produced harmonics just as a conventional one does. On the other hand, the active filter plays a role in improving the filtering characteristics of the passive filter.

L. Chen [44], he suggested that an assessment and comparison of hybrid active filters, including their topologies, ratings, and control algorithms. Simulations are presented, along with a comprehensive topology and performance comparison. In addition, a modified "p-q" theory is introduced for control strategies, which is more feasible for extracting harmonic components for distorted load voltages.

In another proposed technique the APF generates a voltage waveform similar to the voltage harmonics at the load side, but in opposition [60]. This strategy only prevents the parallel passive filter depending on the source impedance. The other limitations of the passive filter nevertheless remain.

Other control strategies combining both the aforementioned have been proposed to improve the parallel passive filter compensation characteristics [63], but they go on suffering the difficulty of finding an appropriate value of gain  $K$ .

L. A. Morán [66], describes different power quality problems in distribution systems and their solutions with power electronics based equipment. Shunt, hybrid and series active power filters are described showing their compensation characteristics and principles of operation. Different power circuits topologies and control scheme for each type of active power filter are analyzed. The compensation characteristics of each topology with the respective control scheme are proved by simulation and experimentally.

J. W. Dixon [104], he has been studied analytically and tested using computer simulations and experiments. In the experiments, it has been verified that the filter keeps the line current almost sinusoidal and in phase with the line voltage supply. It also responds very fast under sudden changes in the load conditions, reaching its steady state in about two cycles of the fundamental.

The control target most used is that provides high impedance for the harmonics while providing zero impedance for the fundamental component. This strategy is achieved when the APF generates the voltage proportional to the source current harmonics [107]-[108]. With this control algorithm, the elimination of series and/or parallel resonance with the rest of the system is possible. The passive filter becomes harmonic drain of the close loads. Besides, it can prevent the compensation features from its independence on the system impedance. From theoretical point of view, the ideal situation would be that the proportionality constant  $K$  between the active filter output voltage and source current harmonics had a high value, at the limit it would be an infinite value. However, this would mean that the control objective is impossible to achieve. The chosen  $K$  value is usually small. It avoids high power active filters. However, the choice of the appropriate  $K$  value is an unsolved question, since it is related to the passive filter and the source impedance values. Besides, his strategy is not suitable to be used in the systems with variable loads because the passive filter reactive power is constant, and therefore, the set compensation equipment and load has variable power factor.

Another approach suggests that the APF generates a voltage, which compensates the passive filter and load reactive power, so it allows the current harmonics to be eliminated [110]. The calculation algorithm is based on the instantaneous reactive power theory [8]. There the control target is to achieve constant power in the source side.

K. V. Kumar [113], have been presented the performance comparison of Shunt Active Power Filter (SAPF) and Hybrid Active Power Filter (HAPF) with three different non linear loads. Two different PI controllers based on average load active power and synchronous reference frame theory are employed in this simulation study. MATLAB/SIMULINK is used for the simulation of SAPF and HAPF.

K. Karthik, St. Johns [114], he proposed a control scheme based on synchronous d-q-0 transformation for a hybrid series voltage compensator. The effectiveness of the new control scheme in compensating for voltage sags, distortion and voltage flickers is demonstrated using simulation results. Its dual role as a harmonic isolator is also described. A comparison between the proposed schemes against an existing control scheme is presented via simulation.

E. R. Ribeiro [115], have been presented a series active filter using a simple control technique. The series active filter is applied as a controlled voltage source contrary to its common usage as variable impedance. It reduces the terminal harmonic voltages, supplying linear or even nonlinear loads with a good quality voltage waveform. The operation principle, control strategy, and theoretical analysis of the active filter are presented.

Hideaki Fujita [116], have already proposed the combined system of a shunt passive filter and a small-rated series active filter. The purpose of the series active filter is to solve such a problem as series and parallel resonance which is inherent in a shunt passive filter used alone.

S. P. Litran [117], he combined system of shunt passive and series active filter for a four-wire three-phase system has been designed and simulated with MATLAB/SIMULINK. The system combined mitigates the source current harmonics and compensates also unbalance voltages reducing the problems of using only a shunt passive filter. Therefore, a new control method based in the power vector theory has been proposed.

Salvador P. Litran [118], he described three different control strategies have been applied to a series active filter. The first is based on that the filter voltage must be proportional to the harmonic of the source current. With the second strategy the filter voltage

must be equal to voltage harmonics on the side load but in opposition. The third strategy is hybrid control where the filter voltage is obtained using both previous strategies.

All the presented strategies are applied to three-phase three-wire system with balanced load. In this thesis control strategy based on the dual formulation of the electric power vectorial theory for non-sinusoidal and unbalanced voltage is proposed. In [105] the same theory is implemented for balance and resistive load. Here an attempt is made to apply the same theory for unbalanced and non-sinusoidal voltage conditions for randomly varying load as an electric arc furnace (EAF).

### 4.3.1 Reference voltage design

Under ideal condition of balanced and sinusoidal voltages, load current at PCC will be proportional to the supply voltage:

$$\bar{v} = R_e \cdot \bar{i} \quad (4.1)$$

Further set of supply quantities-voltage and current vectors of equation (4.1) can be defined as:

$$v = \begin{bmatrix} v_a \\ v_b \\ v_c \end{bmatrix} = [v_a \quad v_b \quad v_c]^T \quad (4.2)$$

$$i = \begin{bmatrix} i_a \\ i_b \\ i_c \end{bmatrix} = [i_a \quad i_b \quad i_c]^T \quad (4.3)$$

Now for three phases three wire system,  $abc$  to  $\alpha\beta$  transformation coordinates obtained:

$$\begin{bmatrix} v_\alpha \\ v_\beta \end{bmatrix} = \sqrt{\frac{2}{3}} \begin{bmatrix} 1 & -\frac{1}{2} & -\frac{1}{2} \\ 0 & \frac{\sqrt{3}}{2} & -\frac{\sqrt{3}}{2} \end{bmatrix} \begin{bmatrix} v_a \\ v_b \\ v_c \end{bmatrix} \quad (4.4)$$

$$\begin{bmatrix} i_\alpha \\ i_\beta \end{bmatrix} = \sqrt{\frac{2}{3}} \begin{bmatrix} 1 & -\frac{1}{2} & -\frac{1}{2} \\ 0 & \frac{\sqrt{3}}{2} & -\frac{\sqrt{3}}{2} \end{bmatrix} \begin{bmatrix} i_a \\ i_b \\ i_c \end{bmatrix} \quad (4.5)$$

Instantaneous real power calculated as:

$$p = v_\alpha \cdot i_\alpha + v_\beta \cdot i_\beta \quad (4.6)$$

Active instantaneous power can also be expressed in vectorial form by means of dot product:

$$p = \begin{bmatrix} i_\alpha & i_\beta \end{bmatrix}^T \cdot \begin{bmatrix} v_\alpha \\ v_\beta \end{bmatrix} \quad (4.7)$$

$$\therefore \bar{p} = \bar{i}_{\alpha\beta}^T \cdot \bar{v}_{\alpha\beta} \quad (4.8)$$

Similarly the reactive instantaneous power can also be expressed in vectorial form by means of dot product:

$$q = v_\alpha \cdot i_\beta - v_\beta \cdot i_\alpha \quad (4.9)$$

$$q = \begin{bmatrix} i_\beta & -i_\alpha \end{bmatrix}^T \cdot \begin{bmatrix} v_\alpha \\ v_\beta \end{bmatrix} \quad (4.10)$$

$$\therefore \bar{q} = \bar{i}_{\alpha\beta\perp}^T \cdot \bar{v}_{\alpha\beta} \quad (4.11)$$

From equations (4.8) & (4.11) it can be written as:

$$\begin{bmatrix} p \\ q \end{bmatrix} = \begin{bmatrix} \bar{i}_{\alpha\beta}^T \\ \bar{i}_{\alpha\beta\perp}^T \end{bmatrix} \cdot \bar{v}_{\alpha\beta} \quad (4.12)$$

In the  $\alpha\beta$  - plane,  $\bar{i}_{\alpha\beta}$  and  $\bar{i}_{\alpha\beta\perp}$  vector establishes two coordinates axes. The voltage vector  $\bar{v}_{\alpha\beta}$  can be decomposed in its orthogonal projection on the axis defined by the currents vectors as shown in Figure 4.2 [105].

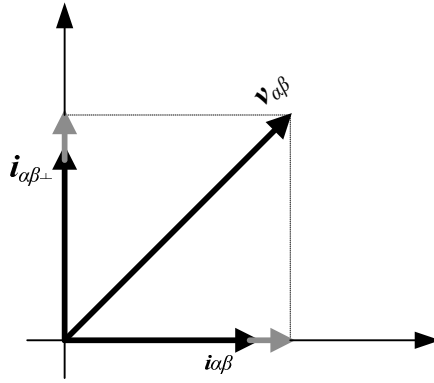


**Figure 4.2 Voltage vector decomposition**

By means of current vectors and the real-imaginary power, the voltage vector can be calculated as:

$$\bar{v}_{\alpha\beta} = \frac{p}{i_{\alpha\beta}^2} \cdot \bar{i}_{\alpha\beta} + \frac{q}{i_{\alpha\beta}^2} \cdot \bar{i}_{\alpha\beta\perp} \quad (4.13)$$

For balanced and sinusoidal currents, average power supplied by the source will be:

$$P_s = I_1^2 \cdot R_e \quad (4.14)$$

It must be clearly understood that when voltage is balanced and sinusoidal, only the fundamental component transports the power consumed by the load.

Now compensator instantaneous power is the difference between the real instantaneous power required by the load and the instantaneous power supplied by the source:

$$p_c(t) = p_L(t) - p_s(t) \quad (4.15)$$

Taking integration on both the side of equation (4.15) yields:

$$\frac{1}{T} \int p_c(t) = \frac{1}{T} \int p_L(t) - \frac{1}{T} \int p_s(t) \quad (4.16)$$

In equation (4.16), the average power exchanged by the compensator has to be null:

$$\therefore P_c = \frac{1}{T} \int p_c(t) \cdot d(t) = 0 \quad (4.17)$$

Substituting equation (4.16) in to equation (4.17) yields:

$$\therefore 0 = \frac{1}{T} \int p_L(t) - \frac{1}{T} \int p_s(t)$$

$$\therefore 0 = P_L - P_s$$

$$\therefore P_L = P_s$$

$$\therefore P_L = I_1^2 \cdot R_e \quad [:\text{equation (4.14)}]$$

$$\therefore R_e = \frac{P_L}{I_1^2} \quad (4.18)$$

The voltage at the series active filter connection point (PCC) in  $\alpha\beta$  coordinates can be calculated by multiplying equation (4.18) by  $\bar{i}_{\alpha\beta}$  on both the sides:

$$R_e \cdot \bar{i}_{\alpha\beta} = \frac{P_L}{I_1^2} \cdot \bar{i}_{\alpha\beta} \quad (4.19)$$

$$\therefore \bar{v}_{PCC\alpha\beta} = \frac{P_L}{I_1^2} \cdot \bar{i}_{\alpha\beta} \quad (4.20)$$

The load voltage calculated according to equation (4.13):

$$\bar{v}_{L\alpha\beta} = \frac{P_L}{i_{\alpha\beta}^2} \cdot \bar{i}_{\alpha\beta} + \frac{Q_L}{i_{\alpha\beta}^2} \cdot \bar{i}_{\alpha\beta\perp} \quad (4.21)$$

The reference signal for the output voltage of the series active filter is given by:

$$\bar{v}_{c\alpha\beta}^* = \bar{v}_{PCC\alpha\beta} - \bar{v}_{L\alpha\beta} \quad (4.22)$$

Substituting equations (4.20) & (4.21) into equation (4.22), we get:

$$\therefore \bar{v}_{c\alpha\beta}^* = \left[ \frac{P_L}{I_1^2} - \frac{p_L}{i_{\alpha\beta}^2} \right] \cdot \bar{i}_{\alpha\beta} - \frac{q_L}{i_{\alpha\beta}^2} \cdot \bar{i}_{\alpha\beta\perp} \quad (4.23)$$

Equation (4.23) gives reference voltage vector for the output of the series active filter under balance and sinusoidal conditions.

Now, for unbalanced and non-sinusoidal currents of EAF  $R_e$  can be refined as:

$$R_e = \frac{P_L}{I_1^{+2}} \quad (4.24)$$

Substituting  $I_1^{+2}$  instead of  $I_1$  in equation (4.23) yields:

$$\bar{v}_{c\alpha\beta}^* = \left[ \frac{P_L}{I_1^{+2}} - \frac{p_L}{i_{\alpha\beta}^2} \right] \cdot \bar{i}_{\alpha\beta} - \frac{q_L}{i_{\alpha\beta}^2} \cdot \bar{i}_{\alpha\beta\perp} \quad (4.25)$$

$$\begin{aligned} \therefore \begin{bmatrix} v_{c\alpha}^* \\ v_{c\beta}^* \end{bmatrix} &= \left[ \frac{P_L}{I_1^{+2}} - \frac{p_L}{(i_\alpha^2 + i_\beta^2)} \right] \cdot \begin{bmatrix} i_\alpha \\ i_\beta \end{bmatrix} - \frac{q_L}{(i_\alpha^2 + i_\beta^2)} \cdot \begin{bmatrix} i_\beta \\ -i_\alpha \end{bmatrix} \\ \therefore \begin{bmatrix} v_{c\alpha}^* \\ v_{c\beta}^* \end{bmatrix} &= \begin{bmatrix} \left( \frac{P_L}{I_1^{+2}} - \frac{p_L}{(i_\alpha^2 + i_\beta^2)} \right) \cdot i_\alpha - \frac{q_L}{(i_\alpha^2 + i_\beta^2)} \cdot i_\beta \\ \left( \frac{P_L}{I_1^{+2}} - \frac{p_L}{(i_\alpha^2 + i_\beta^2)} \right) \cdot i_\beta + \frac{q_L}{(i_\alpha^2 + i_\beta^2)} \cdot i_\alpha \end{bmatrix} \end{aligned} \quad (4.26)$$

Equation (4.26) gives reference signals in  $\alpha\beta$  coordinates for series active filter.

Further simplifying:

$$\therefore v_{c\alpha}^* = \left( \frac{P_L}{I_1^{+2}} - \frac{p_L}{(i_\alpha^2 + i_\beta^2)} \right) \cdot i_\alpha - \frac{q_L}{(i_\alpha^2 + i_\beta^2)} \cdot i_\beta \quad (4.27)$$

$$\therefore v_{c\beta}^* = \left( \frac{P_L}{I_1^{+2}} - \frac{p_L}{(i_\alpha^2 + i_\beta^2)} \right) \cdot i_\beta + \frac{q_L}{(i_\alpha^2 + i_\beta^2)} \cdot i_\alpha \quad (4.28)$$

Taking  $\alpha\beta$  to  $abc$  transformation of equations (4.27)& (4.28), we get:

$$\begin{bmatrix} v_{ca}^* \\ v_{cb}^* \\ v_{cc}^* \end{bmatrix} = \sqrt{\frac{2}{3}} \begin{bmatrix} 1 & 0 \\ -\frac{1}{2} & \frac{\sqrt{3}}{2} \\ -\frac{1}{2} & -\frac{\sqrt{3}}{2} \end{bmatrix} \begin{bmatrix} v_{c\alpha}^* \\ v_{c\beta}^* \end{bmatrix} \quad (4.29)$$

The load and series active filter will behave as a resistor with  $R_e$  value for the reference signal supplied by equation (4.29).

### 4.3.2 Proposed control scheme design

Reference signals indicated by (4.29) are obtained by means of reference calculator shown in Figure 4.3. It is implemented in MATLAB-Simulink. The input signals are the voltage vector measured at the load side and the current vector measured at the source side. By means of calculation block,  $v_{\alpha\beta}$  and  $i_{\alpha\beta}$  vectors in  $\alpha\beta$  coordinates can be calculated. The product of these vectors allows the instantaneous real power and the instantaneous imaginary power to be calculated using equations (4.6) and (4.9). The average value of the instantaneous real power can be obtained with a low-pass filter (LPF). The LPFs are implemented with a Simulink block. This block is the model of a second-order filter, where the cut-off frequency was fixed to 100 Hz and the damping factor to 0.707. It let to reach a settling time of 8 ms.

The average power so obtained is then divided by the average value of the norm of the positive sequence fundamental component of the current vector. For this, the positive-sequence component is calculated by means of the block “Direct-sequence component”, where the Fortescue instantaneous transformation is applied:

$$i^+ = \frac{1}{\sqrt{3}} \cdot (i_a + a \cdot i_b + a^2 \cdot i_c) \quad (4.30)$$

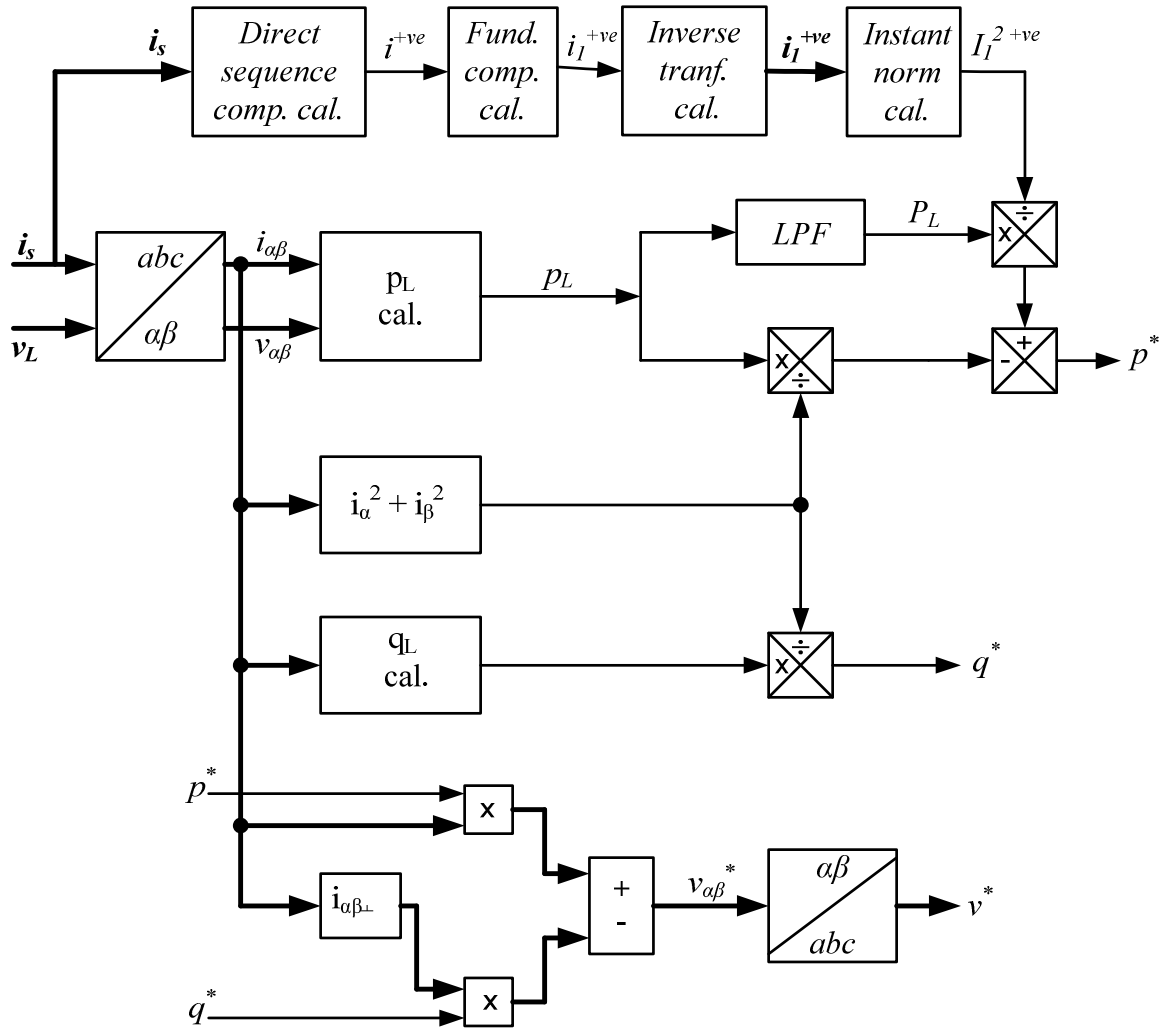
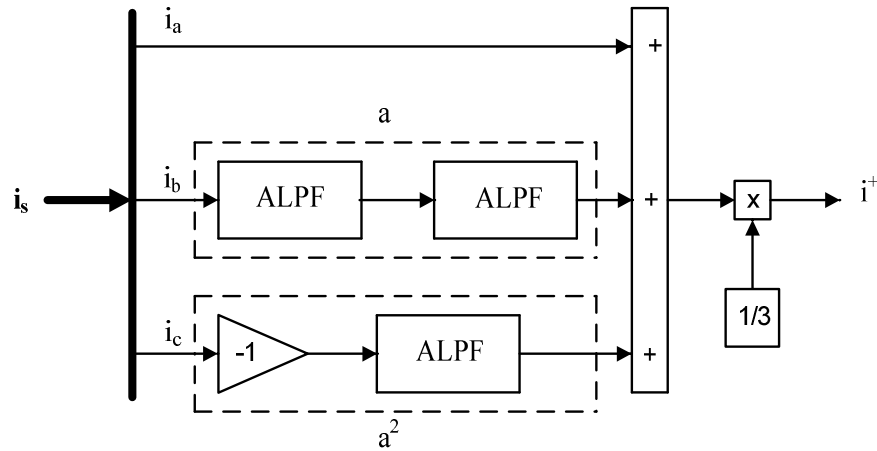


Figure 4.3 Reference signal calculator

In equation (4.30) “ $a$ ” is operator means  $120^\circ$  phase shift, which is defined by:

$$a = e^{j\frac{2\pi}{3}} \quad (4.31)$$

Figure 4.4 shows the calculation scheme to determine the direct sequence component.



**Figure 4.4 Direct-sequence component calculation**

ALPF is an all-pass filter introduces  $60^\circ$  delay at fundamental frequency. Therefore “ $a$ ” operator is achieved by connecting such two ALPF in cascade. “ $a^2$ ” is achieved by inverting the input and connecting single ALPF as shown in Figure 4.4. The ALPF is implemented by means of Simulink transfer function block defined by:

$$F(s) = \frac{s - 181.4}{s + 181.4} \tag{4.32}$$

The fundamental harmonic of current positive sequence component is determined by “*Fund. Comp. cal*” block as shown in Figure 4.5.

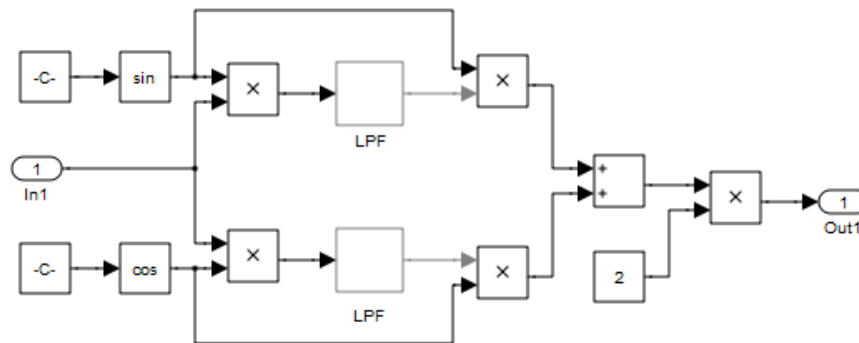


**Figure 4.5 Fundamental positive sequence component calculator**

Each component of the source current vector is multiplied by  $\sin\omega t$  and  $\cos\omega t$ , where  $\omega t$  is the fundamental frequency in rad/sec. The average values are obtained using low pass filters (LPFs). The outputs are again multiplied by  $\sin\omega t$  and  $\cos\omega t$ , and then multiplied by 2.

The Fortescue inverse transformation allows current vector of direct-sequence fundamental component to be obtained. It is calculated by means of following equation:

$$i_1^+ = [i_{1a}^+ \quad i_{1b}^+ \quad i_{1c}^+]^T = [i_{1a}^+ \quad a^2 \cdot i_{1a}^+ \quad a \cdot i_{1a}^+] \quad (4.33)$$

which are the waveforms of the direct-sequence component of the current fundamental component. The calculation scheme is shown in Figure 4.6.

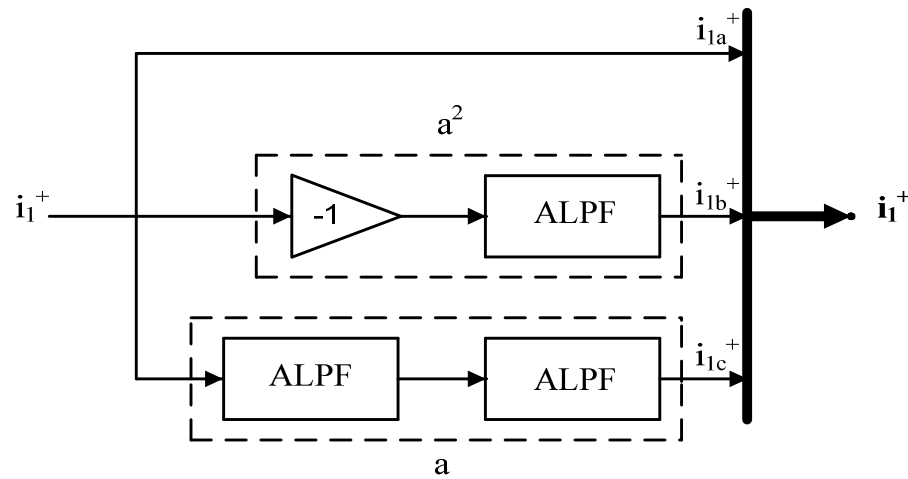


**Figure 4.6 Fortescue inverse transformation**

The norm of the positive-sequence fundamental component of the current vector is defined by (4.34):

$$i_1^{+2} = i_{1a}^{+2} + i_{1b}^{+2} + i_{1c}^{+2} \quad (4.34)$$

Since have the same rms value and each phase shifted by an angle of  $120^\circ$ . This is implemented by the block “instant norm” in the Figure 4.3.

The average power so obtained is then divided by the average value of the norm of the positive sequence fundamental component of the current vector. The real instantaneous

power is then divided by  $i_{\alpha\beta}^2$  as shown in Figure 4.3. The result is multiplied by the current vector  $\bar{i}_{\alpha\beta}$ , which allows the first term in the compensation voltage in (4.23) to be determined. On the other hand, the imaginary instantaneous power is obtained and divided by  $i_{\alpha\beta}^2$  and then multiplied by the current vector  $\bar{i}_{\alpha\beta L}$ . This determines the second term in the compensation voltage in (4.23).

## 4.4 Series APF Simulation

### 4.4.1 IGBT bridge simulation

The compensation voltage has to be generated by a voltage VSI. It uses power transistors; therefore, a PWM generator is necessary. The inverter consists of IGBT bridge as shown in Figure 4.7.

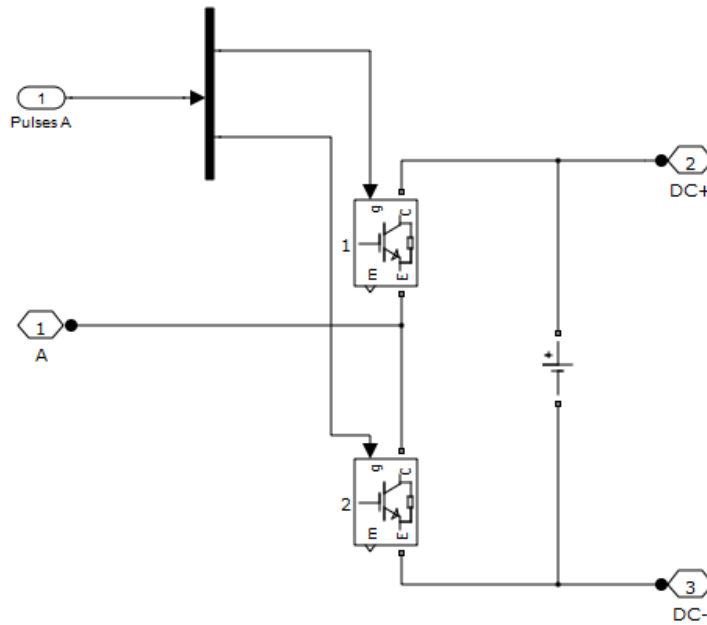


Figure 4.7 IGBT leg for phase-a

On the dc side, a 400 V dc source is connected. Such three sets for three phases are then interfaced at PCC by means of three single phase transformers with a turn ratio of 1:1, as shown in Figure 4.8.

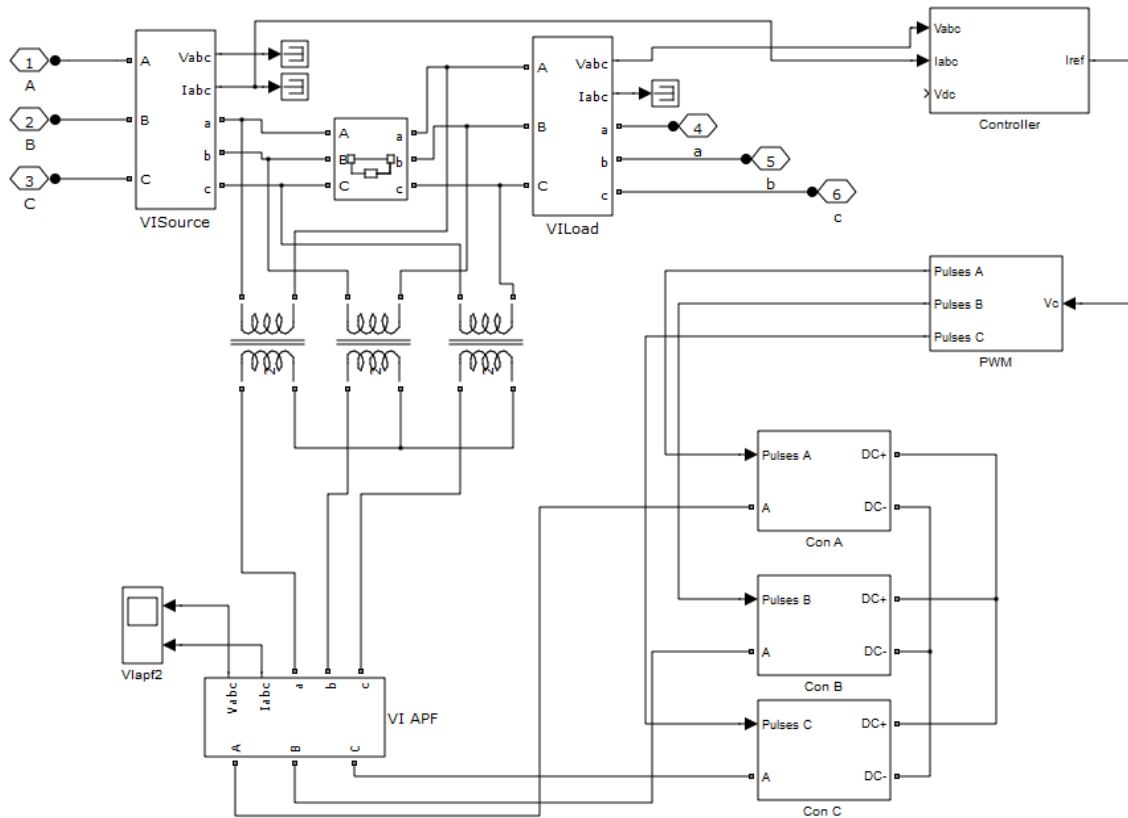


Figure 4.8 Series APF connected at PCC

#### 4.4.2 PWM simulation

The gating signals are generated comparing the reference signal with the inverter output voltage, as shown in Figure 4.9.

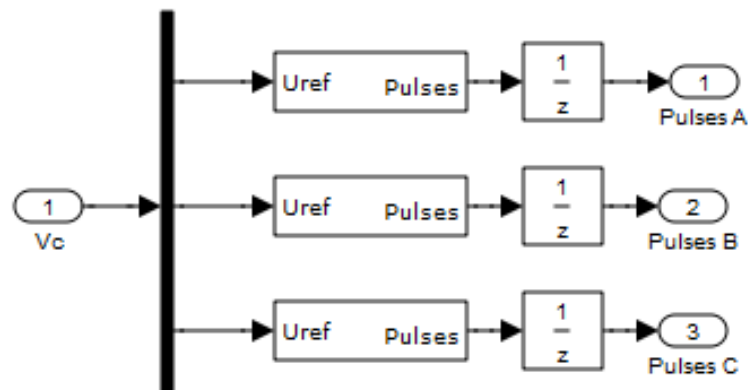


Figure 4.9 Gating signal generation

The PWM Generator block generates pulses for carrier-based pulse width modulation converters using two-level topology. The pulses are generated by comparing a triangular carrier waveform of frequency 5 kHz to a reference modulating signal. The two pulses firing the two devices of a given arm bridge are complementary. The triangular carrier signal is compared with the sinusoidal modulating signal. When the modulating signal is greater than the carrier pulse 1 is high (1) and pulse 2 is low (0). The firing pulses can also be generated by hysteresis control, where the inverter output is directly compared with the reference signals.

### 4.4.3 Proposed control scheme simulation

Figure 4.10 shows simulated Simulink/Matlab file of reference signal calculator.

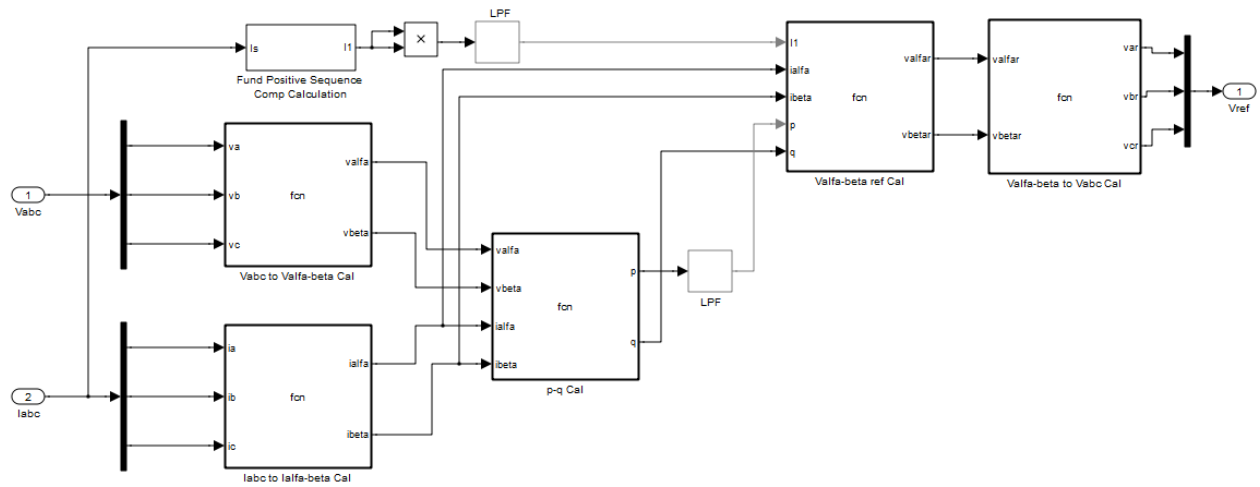


Figure 4.10 Control strategy simulations

## 4.5 State-Space Modeling

### 4.5.1 Main circuit configuration

The system configuration of a CF consists of a series active filter with a shunt passive filter is shown in Figure 4.11.

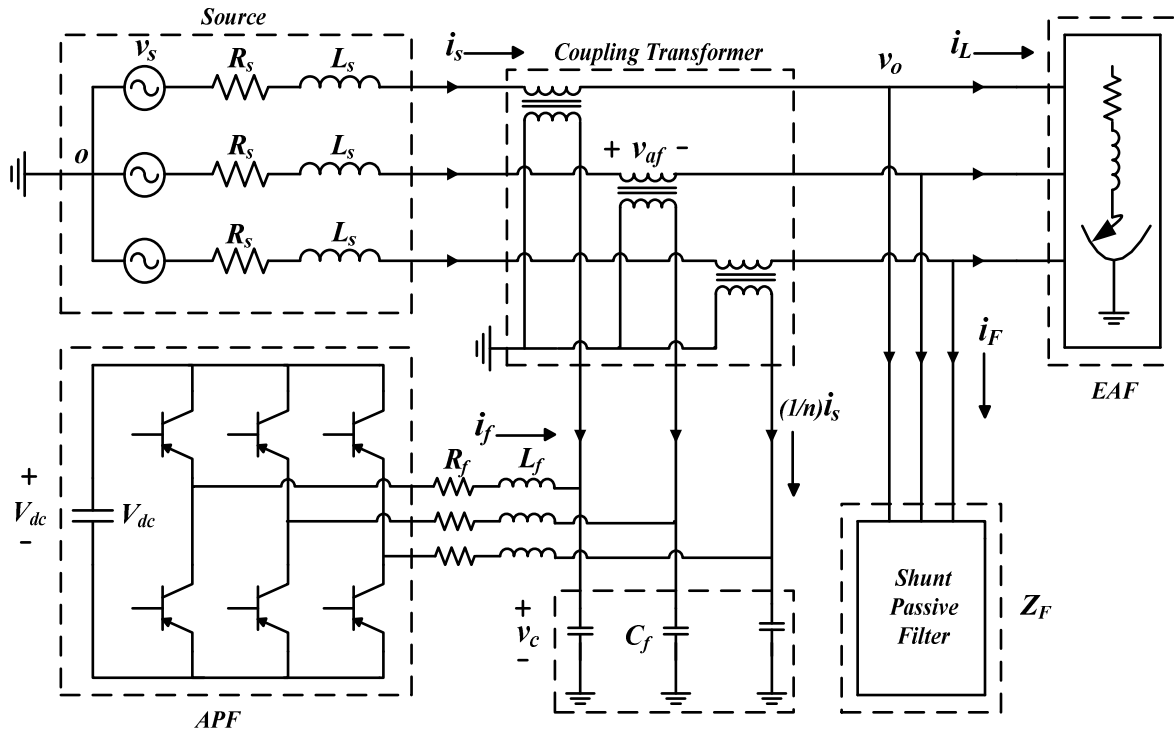


Figure 4.11 Composite filter configuration

It can be divided into four parts:

- An AC mains
- A series active filter
- A Shunt passive filter
- A non-linear load

Series active filter can also be sub-divided into three parts:

- A three phase bridge Inverter (generating harmonic voltage for compensation)
- A second order carrier-wave filter (applied to filter the switching frequency component)
- A coupling transformer (connected between the electric network and the load with transformation ratio=  $n$  )

### 4.5.2 System modeling

The output of voltage of the inverter  $v_c$  changes between  $\pm V_{dc}$  when the IGBTs are switching. The inverter output voltage is represented by:

$$v_c = V_{dc} \cdot (2 \cdot V - 1) \quad (4.35)$$

Where,  $V = [0,1]$ , represents the input discrete values of IGBTs.

The controlled output voltage  $v_c$  so generated will constrain the harmonics produced by the load. The state-space averaged model in the stationary frame of reference is described as follows:

Applying KCL:

$$C_f \cdot \frac{dv_c}{dt} = \frac{1}{n} \cdot i_s + i_f \quad (4.36)$$

Applying KVL:

$$V_{dc} \cdot (2 \cdot V - 1) - i_f \cdot R_f - v_c - L_f \cdot \frac{di_f}{dt} = 0$$

$$\therefore L_f \cdot \frac{di_f}{dt} = [v_c + i_f \cdot R_f - V_{dc} \cdot (2 \cdot V - 1)] \quad (4.37)$$

$$v_s - \frac{1}{n} \cdot v_c - v_o - L_s \cdot \frac{di_s}{dt} = 0$$

$$\therefore L_s \cdot \frac{di_s}{dt} = v_s - \frac{1}{n} \cdot v_c - v_o$$

(4.38)

$$i_s = i_F + i_L = \frac{v_o}{Z_F} + i_L$$

$$\therefore v_o = (i_s - i_L) \cdot Z_F \quad (4.39)$$

$$V = \frac{1}{2} \cdot v_c^*(t) + \frac{1}{2} \quad (4.40)$$

Let the state variables are,

$$x_1 = v_c \Rightarrow \dot{x}_1 = \frac{dv_c}{dt} \quad (4.41)$$

$$x_2 = i_r \Rightarrow \dot{x}_2 = \frac{di_r}{dt} \quad (4.42)$$

$$x_3 = i_s \Rightarrow \dot{x}_3 = \frac{di_s}{dt} \quad (4.43)$$

Re-writing the equations (4.36) to (4.38) using equations (4.41) to (4.43):

$$\dot{x}_1 = 0 \cdot x_1 + \frac{1}{C_f} \cdot x_2 + \frac{1}{n \cdot C_f} \cdot x_3 \quad (4.44)$$

$$\dot{x}_2 = \left( -\frac{1}{L_f} \right) \cdot x_1 + \left( -\frac{R_f}{L_f} \right) \cdot x_2 + 0 \cdot x_3 + \frac{V_{dc}}{L_f} \cdot (2 \cdot V - 1) \quad (4.45)$$

$$\dot{x}_3 = \frac{1}{n \cdot L_s} \cdot x_1 + 0 \cdot x_2 + \left( -\frac{Z_F}{L_s} \right) \cdot x_3 + \left( \frac{v_s}{L_s} + \frac{i_L \cdot Z_F}{L_s} \right) \quad (4.46)$$

The equivalent state-space model can be presented as:

$$\begin{bmatrix} \dot{x}_1 \\ \dot{x}_2 \\ \dot{x}_3 \end{bmatrix} = \begin{bmatrix} 0 & \frac{1}{C_f} & \frac{1}{n \cdot C_f} \\ -\frac{1}{L_f} & -\frac{R_f}{L_f} & 0 \\ \frac{1}{n \cdot L_s} & 0 & \frac{Z_F}{L_s} \end{bmatrix} \begin{bmatrix} x_1 \\ x_2 \\ x_3 \end{bmatrix} + \begin{bmatrix} 0 & 0 & 0 \\ \frac{1}{L_f} & 0 & 0 \\ 0 & \frac{1}{L_s} & \frac{Z_F}{L_s} \end{bmatrix} \begin{bmatrix} V_{dc} \\ v_s \\ i_L \end{bmatrix} \quad (4.47)$$

$$y = x_1 = v_c = \begin{bmatrix} 1 & 0 & 0 \end{bmatrix} \begin{bmatrix} x_1 \\ x_2 \\ x_3 \end{bmatrix} + \begin{bmatrix} 0 & 0 & 0 \end{bmatrix} \begin{bmatrix} V_{dc} \\ v_s \\ i_L \end{bmatrix} \quad (4.48)$$

Equation (4.47) is a state equation and equation (4.48) is an output equation. Comparing them with the standard form,

$$\dot{\bar{x}} = A\bar{x} + B\bar{u} \quad (4.49)$$

$$\bar{y} = C \cdot \bar{x} + D \cdot \bar{u} \quad (4.50)$$

These yields:

$$A = \begin{bmatrix} 0 & \frac{1}{C_f} & \frac{1}{n \cdot C_f} \\ -\frac{1}{L_f} & -\frac{R_f}{L_f} & 0 \\ \frac{1}{n \cdot L_s} & 0 & \frac{Z_F}{L_s} \end{bmatrix} \quad (4.51)$$

$$B = \begin{bmatrix} 0 & 0 & 0 \\ \frac{1}{L_f} & 0 & 0 \\ 0 & \frac{1}{L_f} & \frac{Z_F}{L_s} \end{bmatrix} \quad (4.52)$$

$$C = \begin{bmatrix} 1 & 0 & 0 \end{bmatrix} \quad (4.53)$$

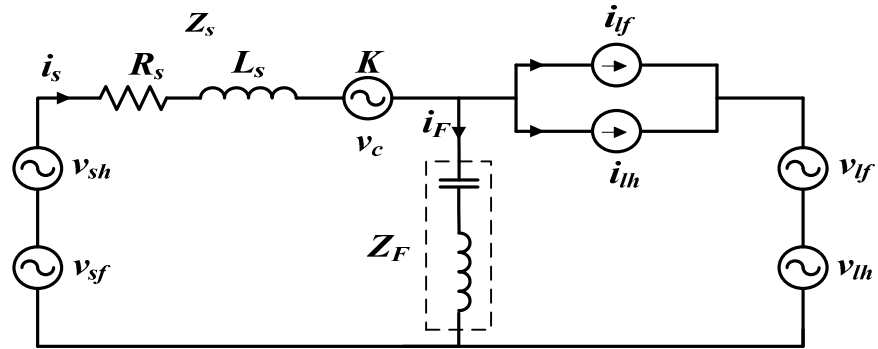
$$D = \begin{bmatrix} 0 & 0 & 0 \end{bmatrix} \quad (4.54)$$

Now Transfer Function of the system is given by:

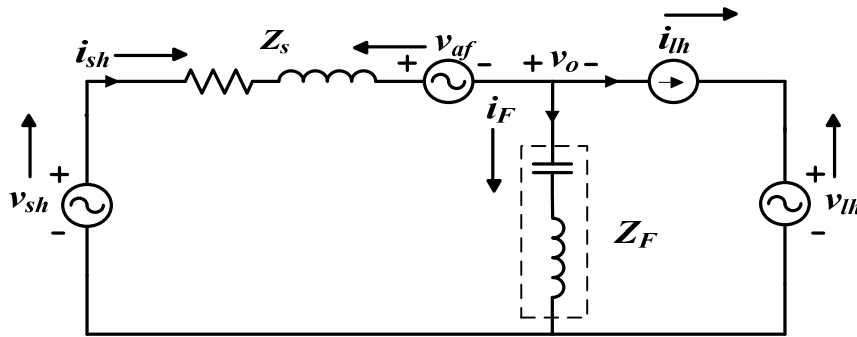
$$G(s) = C[sI - A]^{-1}B + D \quad (4.55)$$

### 4.5.3 System stability analysis

Figure 4.12 (a) shows an equivalent single-phase circuit of the system considering current and voltage harmonics produced by EAF.



(a)



(b)

**Figure 4.12 Single phase equivalent circuit EAF supplying network (a) with fundamental and harmonic components (b) with only harmonic components**

Figure 4.12 (b) shows single-phase equivalent harmonic circuit of system under consideration. The EAF is represented by harmonic current and harmonic voltage source. From the equivalent circuit shown in Figure 4.12(b), it is obtained:

$$v_o = (i_{sh} - i_{lh}) \cdot Z_F \quad (4.52)$$

$$v_{af} = K \cdot i_{sh} \quad (4.57)$$

Applying KVL:

$$v_{sh} - i_{sh} \cdot Z_s - v_{af} - v_o - v_{lh} = 0$$

$$\therefore v_{sh} - i_{sh} \cdot Z_s - (K \cdot i_{sh}) - (i_{sh} - i_{lh}) \cdot Z_{F_o} - v_{lh} = 0$$

$$\therefore v_{sh} - i_{sh} \cdot Z_s - K \cdot i_{sh} - i_{sh} \cdot Z_F + i_{lh} \cdot Z_F - v_{lh} = 0$$

$$\therefore (v_{sh} - v_{lh}) - i_{sh} (Z_s + K + Z_F) + i_{lh} \cdot Z_F = 0$$

$$\therefore i_{sh} = \frac{(v_{sh} - v_{lh})}{(Z_s + K + Z_F)} + \frac{Z_F}{(Z_s + K + Z_F)} \cdot i_{lh} \quad (4.58)$$

With respect to the performance of the compensation, the system behaves like a closed-loop control system. Equation (4.58) can be represented by traditional closed-loop model of composite filter as shown in Figure 4.13 (a).

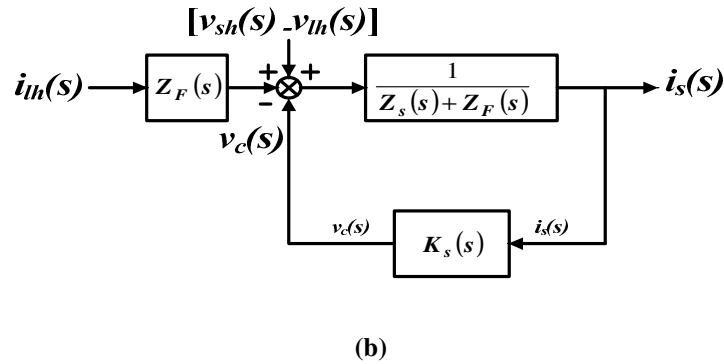
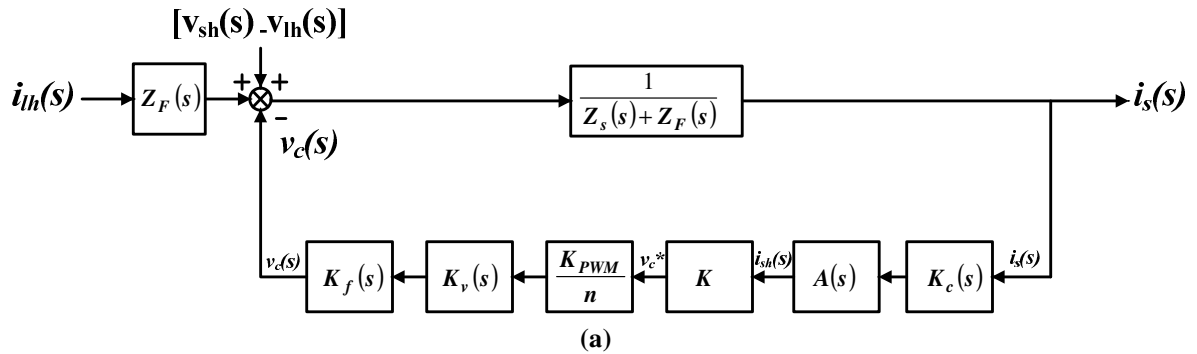


Figure 4.13 Closed loop model for composite filter (a) complete model (b) reduced model

The analysis in the 's' domain could be developed with the help of reduced block diagram shown in Figure 4.13 (b).

The open-loop transfer function  $k(s)$  from input source current to output voltage can be obtained as:

$$k(s) = \frac{v_c(s)}{I_s(s)} = k_c(s) \cdot A(s) \cdot \frac{K_{PWM}}{n} \cdot k_v(s) \cdot k_f(s) \quad (4.59)$$

$$\text{Here, } k_c(s) = \frac{k_c}{T_c \cdot s + 1}$$

$$A(s) = \frac{s^2 + \omega^2}{s^2 + m \cdot s + \omega^2}$$

$k_v(s) = \frac{k_v}{T_v \cdot s + 1}$ , generally  $T_v = \frac{1}{5}$  of carrier wave period (neglecting the sidebands of the switching frequency and the dead time).

$$k_f(s) = \frac{R_f \cdot C_f \cdot s}{L_f \cdot C_f \cdot s^2 + R_f \cdot C_f \cdot s + 1}, \text{ it can be alternatively expressed as:}$$

$$k_f(s) = \frac{1}{T^2 \cdot s^2 + 2 \cdot \xi \cdot T \cdot s + 1}, \text{ where } T = \sqrt{L_f \cdot C_f}$$

Here  $\xi$  controls the shape of the transfer function in the vicinity of the  $f_0 = \frac{1}{2 \cdot \pi \cdot T}$

$$L_f = \frac{n \cdot k}{2 \cdot \pi \cdot f_v} \quad (4.60)$$

$$\text{Here, } k = \left( \frac{3 \cdot V_L^2}{S_L} \right)$$

$$f_{cf} = \frac{1}{2 \cdot \pi \cdot \sqrt{L_f \cdot C_f}} \Rightarrow C_f = \frac{1}{(2 \cdot \pi)^2 \cdot L_f \cdot (f_{cf})^2} \quad (4.61)$$

Here,  $f_{cf} = \frac{f_v}{10}$ , and

$$\xi = \frac{R_f}{2} \cdot \sqrt{\frac{C_f}{L_f}} \Rightarrow R_f = 2 \cdot \xi \cdot \sqrt{\frac{L_f}{C_f}} \quad (4.62)$$

Where, value of  $\xi$  is chosen between 0.4 to 0.6.

$$\therefore 1.6 \sqrt{\frac{L_f}{C_f}} \leq R_f \leq 0.8 \sqrt{\frac{L_f}{C_f}} \quad (4.63)$$

A three-phase 550/50 Hz, 100 MVA power rating an electric arc furnace is considered as a non-linear load. The EAF distribution network parameters are tabulated in Table 4.1.

**Table 4.1 EAF distribution network parameter**

Item	Parameter	Value
Source	V(V)	550
	f(Hz)	50
	$R_s$ ( $\Omega$ )	0.1
	$L_s$ (mH)	0.23
EAF Cable	$R_c$ (m $\Omega$ )	0.38
	$L_c$ ( $\mu$ H)	8.589
APF	$V_{dc}$ (V)	400

The detailed specifications are as follows:

**Table 4.2 CF control parameter**

Parameter	Value
$f_v$ (kHz)	25
$n$	25
$\xi$	0.6
$k_c$	0.2
$\tau_c$ ( $\mu$ s)	100
$k_v$	80
$\tau_v$ ( $\mu$ s)	8
$m$	100
$K_{PWM}$	200/16

Neglecting Kelvin's effect, eddy current effect and attenuation of filter's gain, using (4.60) to (4.63) the maximum gain can be calculated as:

$$k = \left( \frac{3 \cdot V^2}{S} \right) = 3 \cdot \left( \frac{\left( \frac{550}{\sqrt{3}} \right)^2}{10^7} \right) = 0.0303$$

$$k_c(s) = \frac{k_c}{\tau_c \cdot s + 1} = \frac{0.2}{100 \times 10^{-6} \cdot s + 1} = \frac{0.2}{1 \times 10^{-4} \cdot s + 1}$$

$$A(s) = \frac{s^2 + \omega^2}{s^2 + m \cdot s + \omega^2} = \frac{s^2 + (2 \cdot \pi \cdot 50)^2}{s^2 + 100 \cdot s + (2 \cdot \pi \cdot 50)^2} = \frac{s^2 + 314^2}{s^2 + 100 \cdot s + 314^2}$$

$$k_v(s) = \frac{k_v}{T_v \cdot s + 1} = \frac{40}{8 \times 10^{-6} \cdot s + 1}$$

$$L_f = \frac{n \cdot k}{2 \cdot \pi \cdot f_v} = \frac{25 \times 0.03025}{2 \cdot \pi \cdot 25 \times 10^3} = 4.8144 \times 10^{-6} \text{ H}$$

$$C_f = \frac{1}{(2 \cdot \pi)^2 \cdot L_f \cdot (f_{cf})^2} = \frac{1}{(2 \cdot \pi)^2 \cdot (4.816 \times 10^{-6}) \cdot \left(\frac{25 \times 10^3}{10}\right)^2} = 8.4181 \times 10^{-4} \text{ F}$$

$$R_f = 2 \cdot \xi \cdot \sqrt{\frac{L_f}{C_f}} = 2 \cdot (0.6) \cdot \sqrt{\frac{4.816 \times 10^{-6}}{8.424 \times 10^{-4}}} = 0.0908 \text{ } \Omega$$

$$\begin{aligned} k_f(s) &= \frac{R_f \cdot C_f \cdot s}{L_f \cdot C_f \cdot s^2 + R_f \cdot C_f \cdot s + 1} \\ &= \frac{(0.09073) \cdot (8.424 \times 10^{-4}) \cdot s}{(4.816 \times 10^{-6}) \cdot (8.424 \times 10^{-4}) \cdot s^2 + (0.09073) \cdot (8.424 \times 10^{-4}) \cdot s + 1} \\ &= \frac{(7.639 \times 10^{-5}) \cdot s}{(4.053 \times 10^{-9}) \cdot s^2 + (7.639 \times 10^{-5}) \cdot s + 1} \end{aligned}$$

Finally the feedback path transfer function given by (4.59):

$$\begin{aligned} k_s(s) &= \frac{0.2}{1 \times 10^{-4} \cdot s + 1} \cdot \frac{s^2 + 314^2}{s^2 + 100 \cdot s + 314^2} \cdot \frac{200}{16} \cdot \frac{40}{8 \times 10^{-6} \cdot s + 1} \\ &\cdot \frac{(7.639 \times 10^{-5}) \cdot s}{(4.053 \times 10^{-9}) \cdot s^2 + (7.639 \times 10^{-5}) \cdot s + 1} \end{aligned} \quad (4.64)$$

As per [107], the time constant of leading compensator can be calculated as:

$$K_p = \frac{(4.053 \times 10^{-9})}{(7.639 \times 10^{-5})} = 0.530 \times 10^{-4}$$

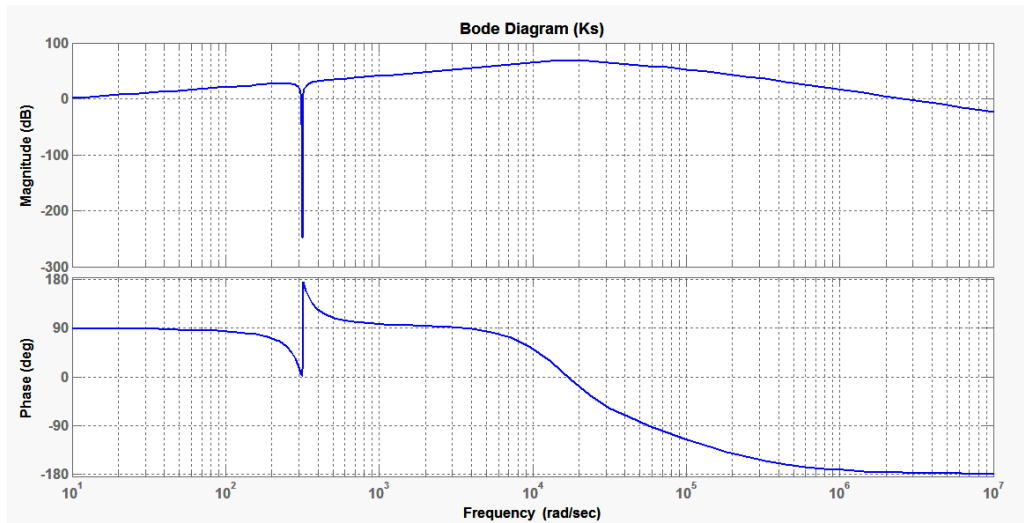
Transfer function of phase-lead compensator can be given by:

$$K_p(s) = 0.530 \times 10^{-4} \cdot s + 1 \quad (4.65)$$

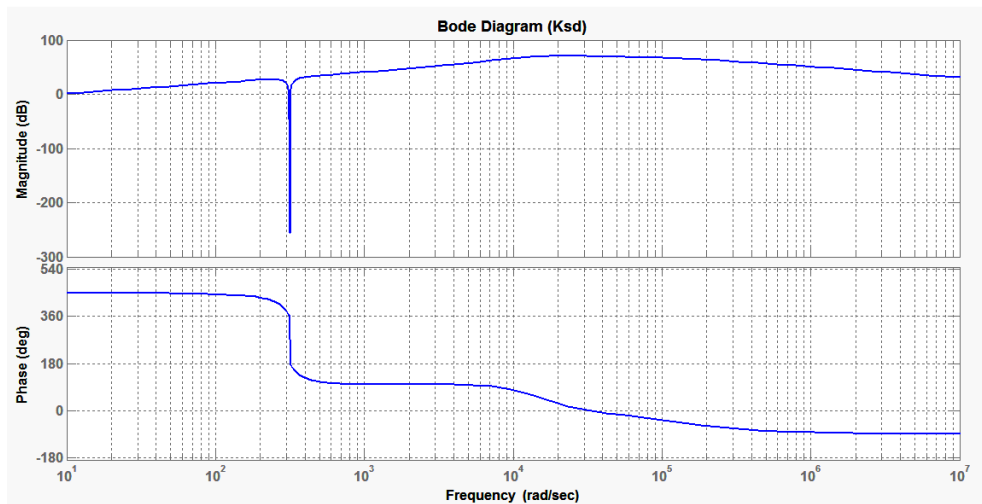
Now the transfer function of feedback path with phase-lead compensator can be given by:

$$K'_s(s) = (0.530 \times 10^{-4} \cdot s + 1) \cdot K_s(s) \quad (4.66)$$

Simulation results of Bode plot for functions  $k_s(s)$  and  $k'_s(s)$  are obtained by (4.65) and (4.66) are shown in Figure 4.14. Figure 4.14 (a) shows magnitude and phase Bode plot for function  $k_s(s)$  and Fig. 4.14 (b) that of function  $k'_s(s)$ . Comparison of simulated results shown in Figure 4.14 (a) with Figure 4.14 (b) shows that the gain margin and the phase margin of the open loop transfer function has improved a lot. Also, the cut-off frequency boosted when, the lead compensation is adopted. Quantified results of gain margin and phase margin are tabulated in Table 4.3.



(a)



(b)

Figure 4.14 Magnitude and phase Bode plot for (a) function  $k_s(s)$  (b) for function  $k'_s(s)$

It can be seen that the gain margin and the phase margin has increased considerably by lead compensation strategy.

**Table 4.3 Bode plot output for open loop transfer functions**

<b>Parameter</b>	<b>Gain margin (dB)</b>	<b>Phase margin (deg)</b>
$k_s(s)$	0.506	1.45
$k'_s(s)$	50.1	40.9

## 4.6 Summary

This chapter describes design of composite filter for power quality improvement of electrical electric arc furnace distribution network. At first, basic compensation principle of composite filter is discussed. Secondly, a control strategy for a composite filter, which is connected with the existing passive filter, is proposed for taking care of the unbalance, non-sinusoidal and randomly varying EAF. The control strategy is based on the dual vectorial theory of power. Next, a state-space averaging model has been constructed to analyze the stability of CF used for PQ improvement of EAF distribution network. It is difficult to obtain a better filter performance confined to the system stability by the traditional control strategy, taking into account the time delay in the control circuit. The analysis has indicated that the time delay can cause a stability problem. Therefore, a phase-lead compensation strategy has been proposed to eliminate the effect of time delay. It suggests method of lead compensation to increase the value of the cut-off frequency. Increase in phase margin has indicated that the proposed control strategy improves the system stability compared with the traditional control strategy. Simulation verifies the validity of the developed theory.

# 5 Application of Composite Filter for PQ issues in Distribution Network

## 5.1 Introduction

This chapter deals with an application of composite filter to EAF distribution network for PQ issues using Matlab-Simulink platform to verify the proposed control. Each power device has been modeled using the SimPowerSystem toolbox library.

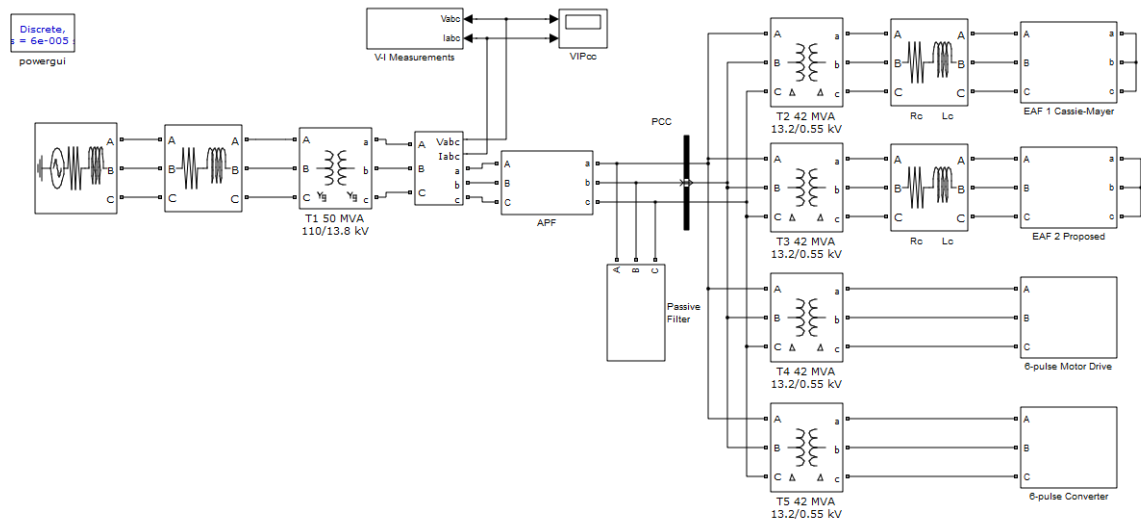


**Figure 5.1 Complete MATLAB simulation file of composite filter connected to EAF network**

Figure 5.1 shows complete Simulink/MATLAB file of test system shown in Figure 2.46. The distribution network consists of EAF-1-Cassie-Mayer model and EAF-2-Proposed model along with the auxiliaries. EAF is modeled as a non-linear time varying voltage controlled source using subsystem/MATLAB. The arc current is taken as the input parameter to this function and the output is non-linear time varying voltage.

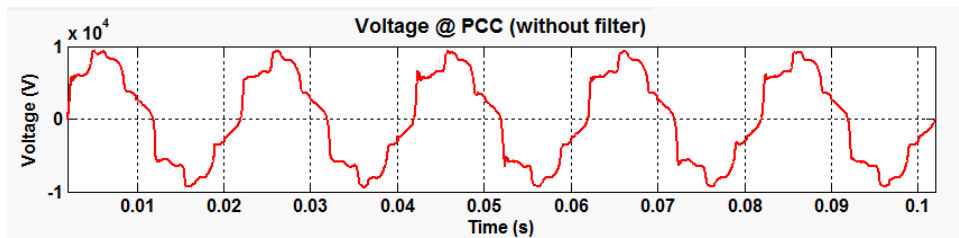
## 5.2 Performance analysis of CF

Performance evaluation of CF for PQ issues in an EAF connected distribution network is carried out for various operational cycles of the EAF, which includes-analysis in refining

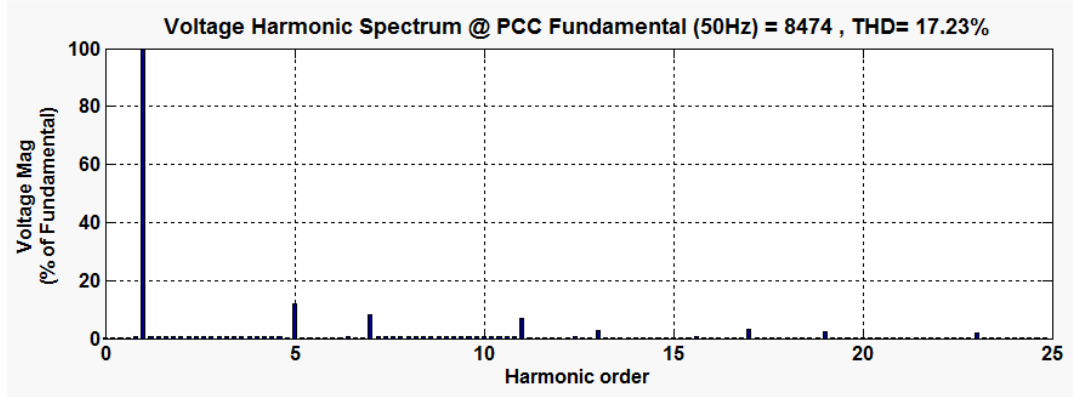
cycle, analysis in melting cycle (sinusoidal flicker), analysis in melting cycle (random cycle) and unbalanced voltage analysis. The performance of EAF in various cycles is discussed in the following sub-sections:

### 5.2.1 Performance analysis of CF in refining cycle

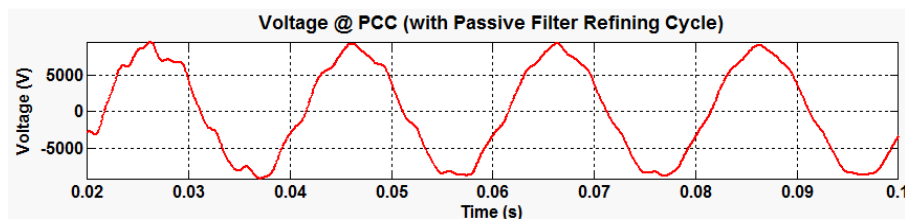
Figure 5.2 shows filter performance in refining cycle of the EAF connected distribution network. Figure 5.2 (a)-(c)-(e) shows  $V_{PCC}$  waveforms without filter, with PF and with CF respectively. Figure 5.2 (b)-(d)-(f) shows harmonic spectrum of  $V_{PCC}$  without filter, with PF and with CF respectively.



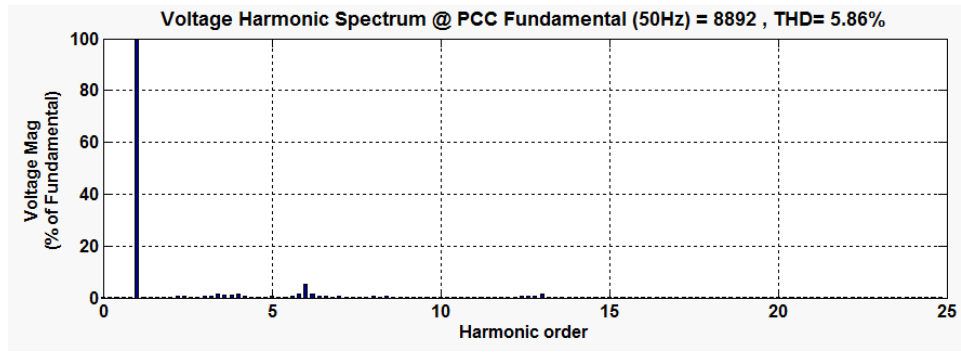
(a)



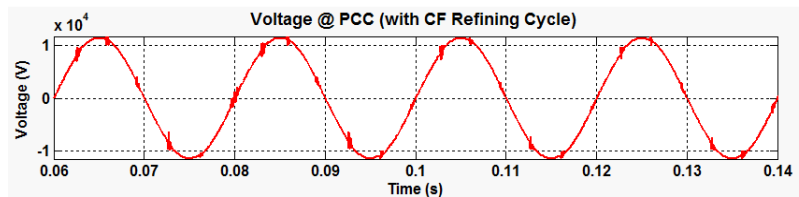
(b)



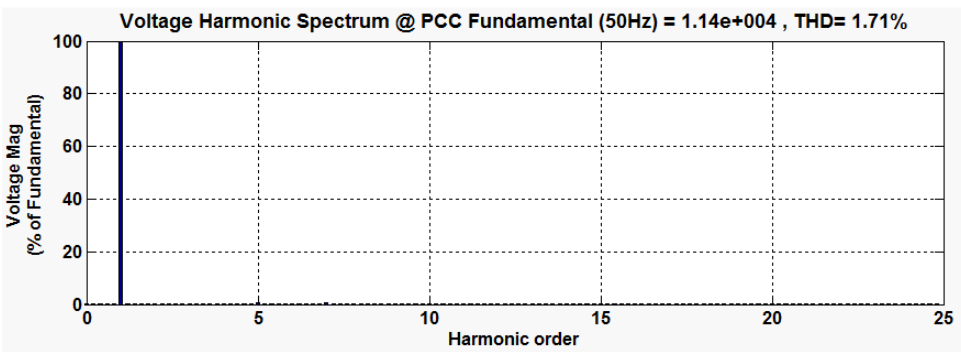
(c)



(d)



(e)



(f)

**Figure 5.2 Filter performance in EAF refining cycle (a)  $V_{PCC}$  without filter (b) harmonic spectrum without filter (c)  $V_{PCC}$  with PF (d) harmonic spectrum with PF (e)  $V_{PCC}$  with CF (f) harmonic spectrum with CF**

The total harmonic distortion of voltage ( $THD_V$ ) observed at PCC is 17.23 % without filter in refining cycle of EAF connected distribution network as shown in Figure 5.2 (b). This value is violating IEEE 519-1992 limits. It should be below 5%. That is improved to 5.86 % after passive filter application as shown in Figure 5.2(d), which is still violating IEEE 519-1992. Application of CF changes  $THD_V$  to 1.71 % as shown in Figure 5.2 (f).

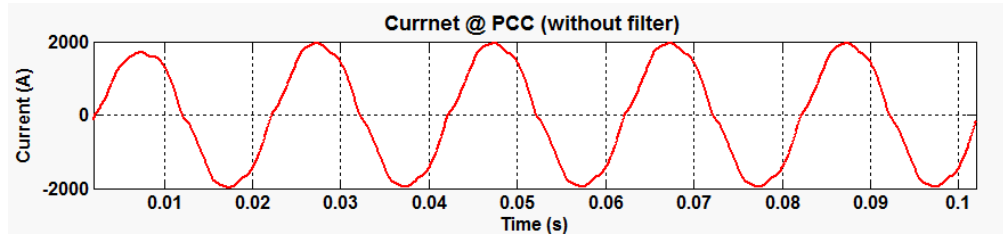
Table 5.1 shows three phase harmonic spectrum details of voltage and current at PCC for refining cycle of the EAF connected distribution network.

**Table 5.1 Harmonic analysis of EAF connected distribution network in refining cycle**

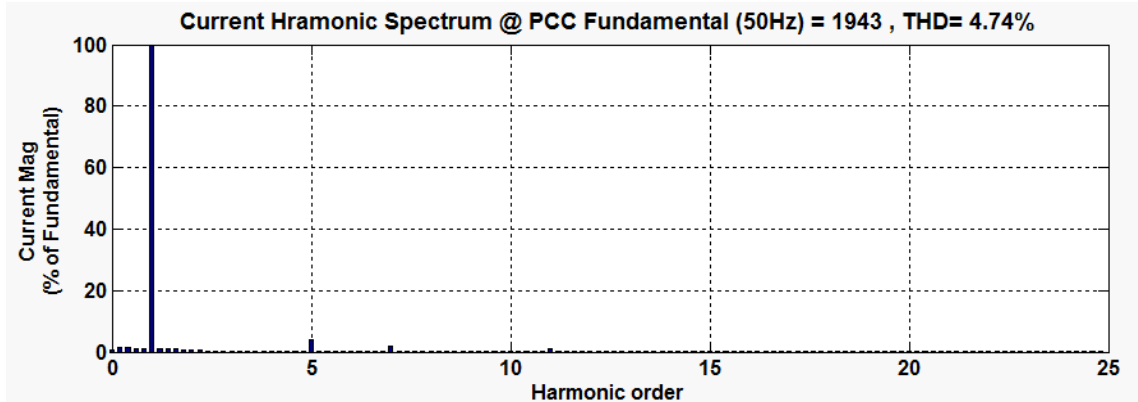
Parameters/condition	Phase	V/I	THD (%)	RMS	Fund.	H <sub>5</sub> (%)	H <sub>7</sub> (%)	H <sub>11</sub> (%)	H <sub>13</sub> (%)
Without filter	Phase-a	V	17.23	5992	8474	11.99	8.27	6.98	2.59
		I	4.74	1374	1943	4.06	2	0	0
	Phase-b	V	17.49	5976	8451	12.29	8.36	7.24	2.73
		I	4.73	1387	1962	4.11	2	1.1	0
	Phase-c	V	17.47	5979	8456	12.26	8.31	7.28	2.73
		I	4.72	1388	1963	4.09	1.99	1.1	0
With PF	Phase-a	V	5.86	6288	8892	0.58	0.47	0.09	1.26
		I	1.72	1413	1999	0.18	0.11	0	0
	Phase-b	V	2.73	6271	8869	0.65	0.33	0.11	0.94
		I	0.82	1413	1997	0.22	0.05	0	0
	Phase-c	V	4.96	6292	8898	0.68	0.23	0.07	0.54
		I	1.54	1405	1987	0.25	0.06	0	0
With CF	Phase-a	V	1.71	8064	1140	0.64	0.44	0.21	0.18
		I	3.88	106.3	150.3	3.33	1.68	0.52	0.31
	Phase-b	V	1.92	8067	11410	0.67	0.44	0.24	0.16
		I	4.33	105.1	148.6	3.74	1.76	0.61	0.35
	Phase-c	V	1.92	8067	11410	0.65	0.43	0.24	0.13
		I	4.29	105.1	148.7	3.6	1.77	0.69	0.3

It can be seen that 5<sup>th</sup>, 7<sup>th</sup>, 11<sup>th</sup> and 13<sup>th</sup> are the major harmonic components present in voltage at PCC. H<sub>5</sub>, H<sub>7</sub> and H<sub>11</sub> are more than IEEE 519-1992 limit of 5 % of harmonic distortion. It can be seen from Table 5.2 that both PF and CF can suppress individual harmonic components within the limit in refining cycle of EAF distribution network at PCC.

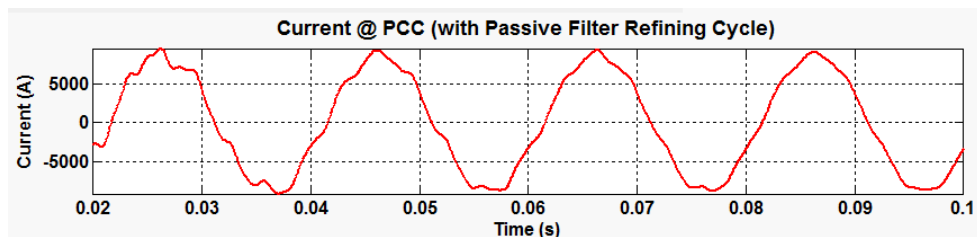
Figure 5.3 shows filter performance in refining cycle of the EAF connected network. Figure 5.3 (a)-(c)-(e) shows  $I_{PCC}$  waveforms without filter, with PF and with CF respectively. Figure 5.3 (b)-(d)-(f) shows harmonic spectrum of  $I_{PCC}$  without filter, with PF and with CF respectively.



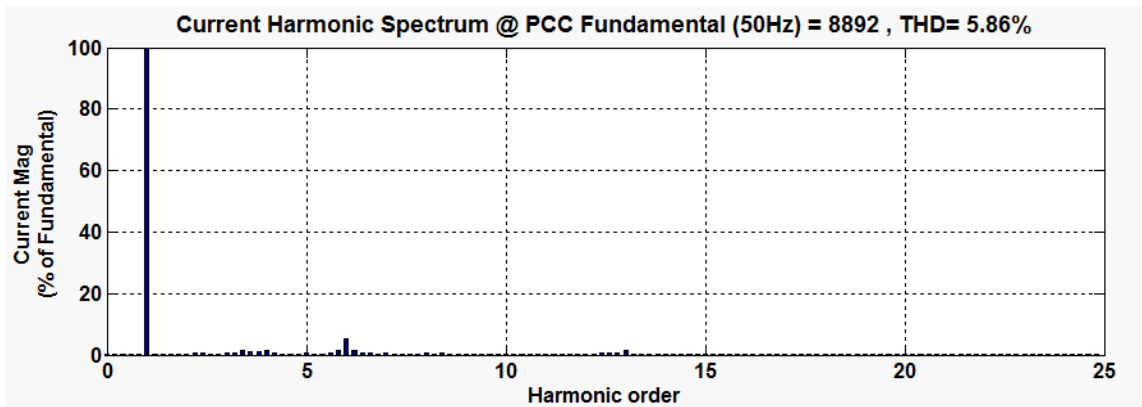
(a)



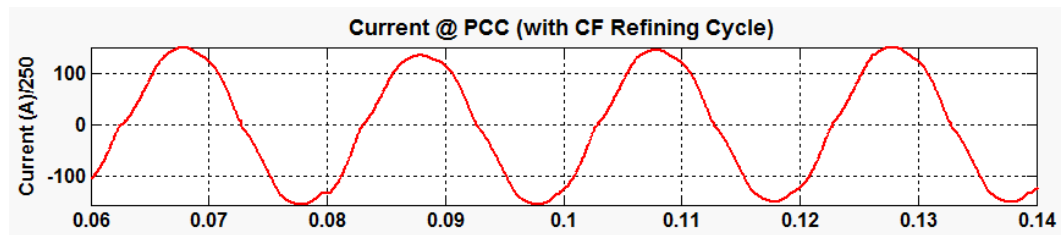
(b)



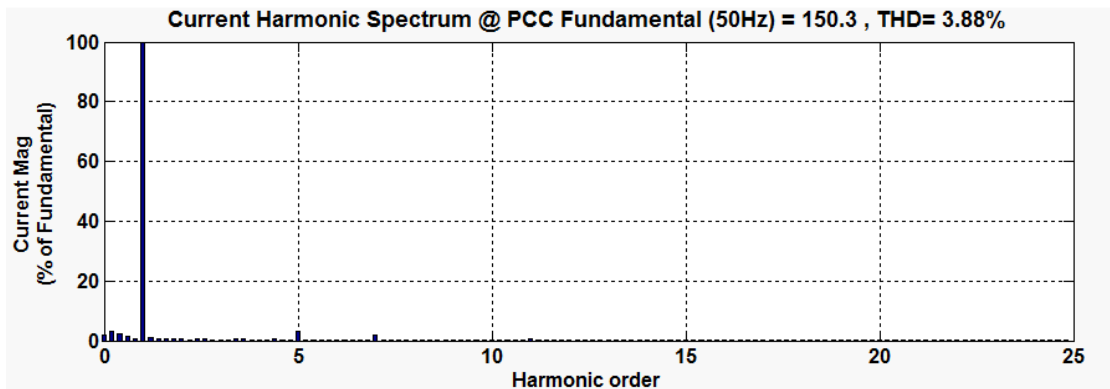
(c)



(d)



(e)



(f)

Figure 5.3 Filter performance in EAF refining cycle (a)  $I_{PCC}$  without filter (b) harmonic spectrum without filter (c)  $I_{PCC}$  with PF (d) harmonic spectrum with PF (e)  $I_{PCC}$  with CF (f) harmonic spectrum with CF

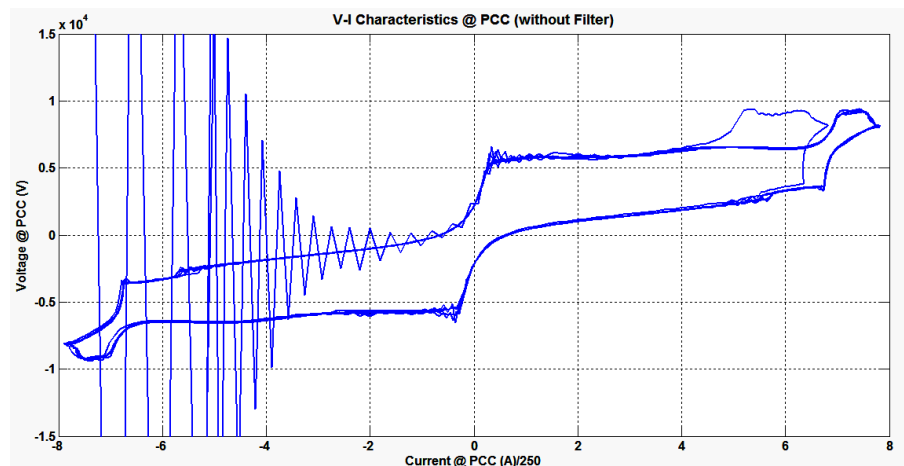
The total harmonic distortion of current ( $THD_I$ ) observed at PCC is 4.74 % without filter in refining cycle of EAF connected distribution network as shown in Figure 5.3 (b). It has improved to 1.72 % and then changes to 3.82 % after PF and CF application as shown in Figure 5.3 (d) and (f) respectively, which are within the permissible limits. Harmonics

spectrum quantified detail is tabulated in Table 5.1. It shows that PF performs better than CF in reducing  $THD_1$  in refining cycle.

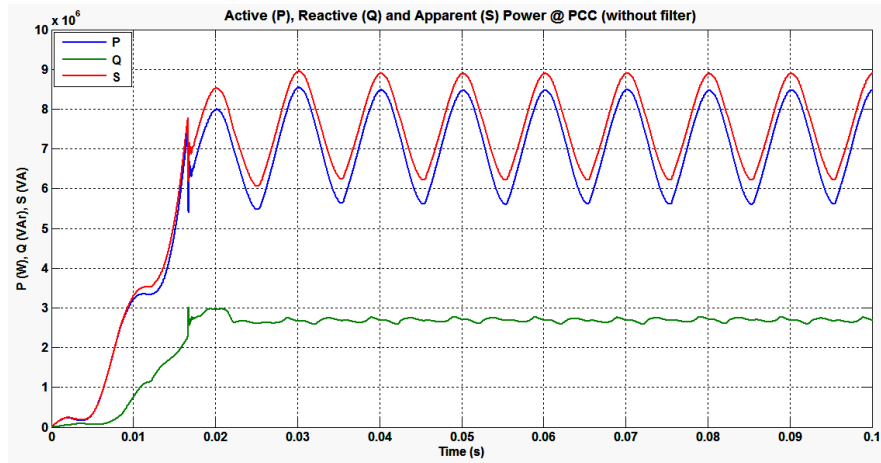
It can be noted that 5<sup>th</sup>, 7<sup>th</sup>, 11<sup>th</sup> and 13<sup>th</sup> are the major harmonic components present in current at PCC.  $H_5$ ,  $H_7$  and  $H_{11}$  are more than IEEE 519-1992 limit of 5 % of harmonic distortion. It can be seen that 5<sup>th</sup>, 7<sup>th</sup>, 11<sup>th</sup> and 13<sup>th</sup> are the major harmonic components present in voltage at PCC.  $H_5$  is more than IEEE 519-1992 limit of 5 % of harmonic distortion.

It can be seen from Table 5.1 that both PF and CF can suppress individual harmonic component within the limit in refining cycle of EAF distribution network at PCC

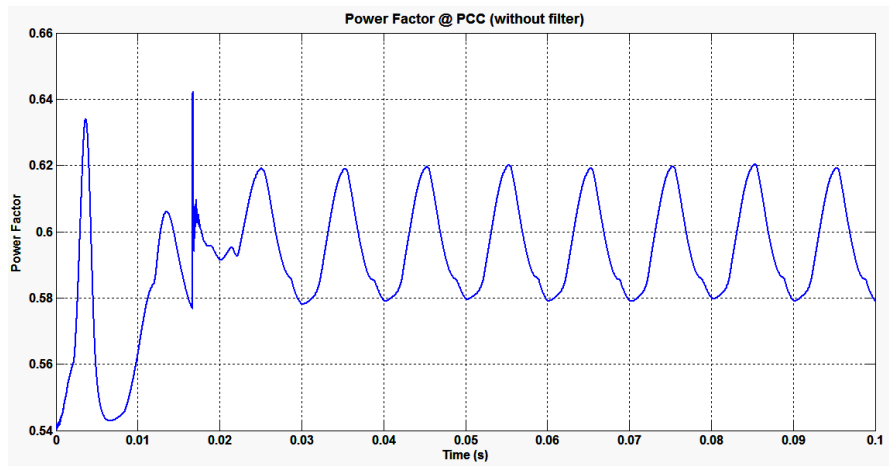
Figure 5.4 (a)-(d)-(g) depicts typical VICs without filter, with PF and with CF application respectively. Figure 5.4 (b)-(e)-(h) shows active-reactive-apparent power consumption at PCC by the EAF distribution network without filter, with PF and with CF application respectively.



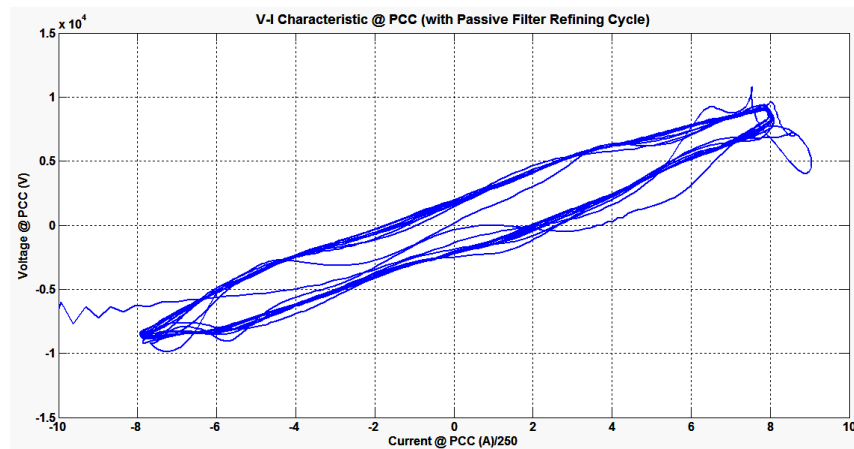
(a)



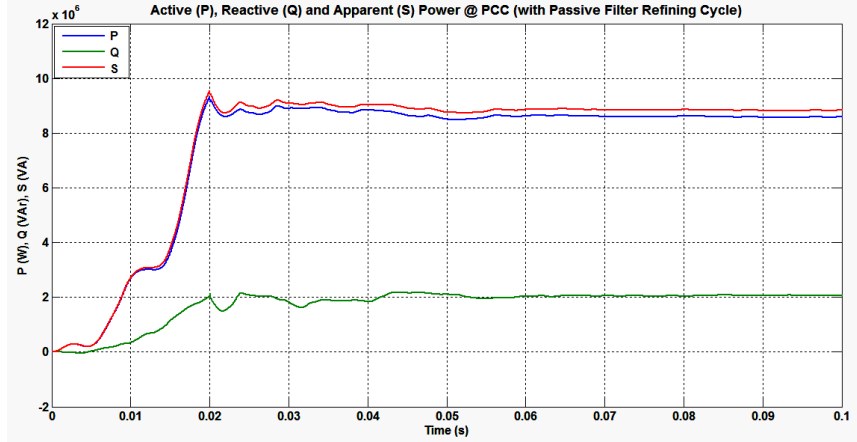
(b)



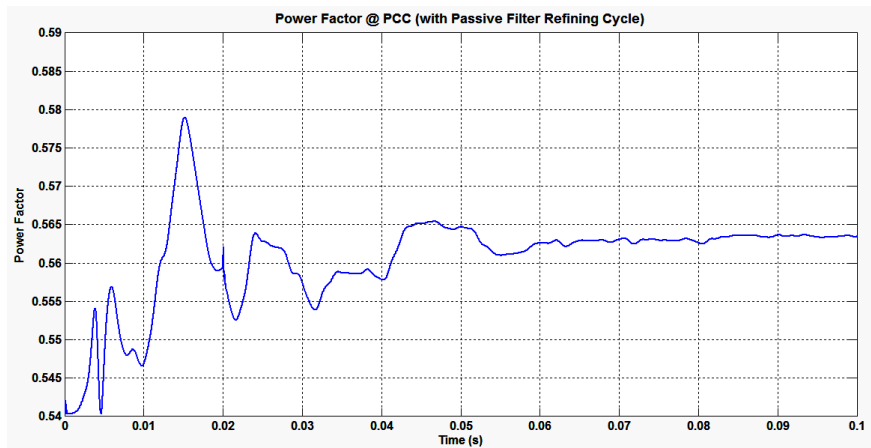
(c)



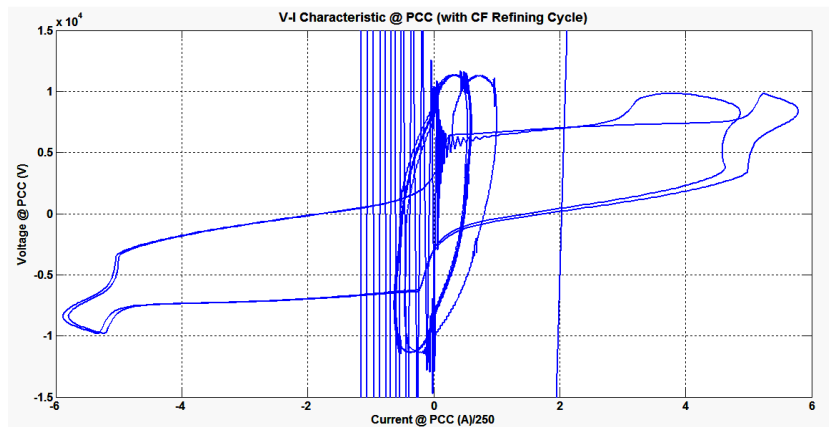
(d)



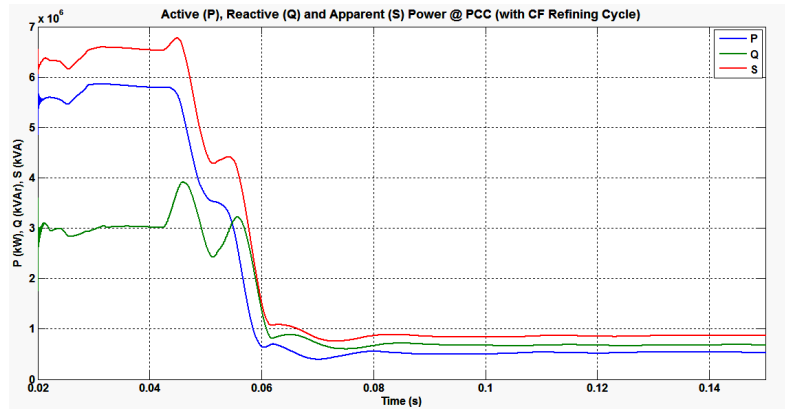
(e)



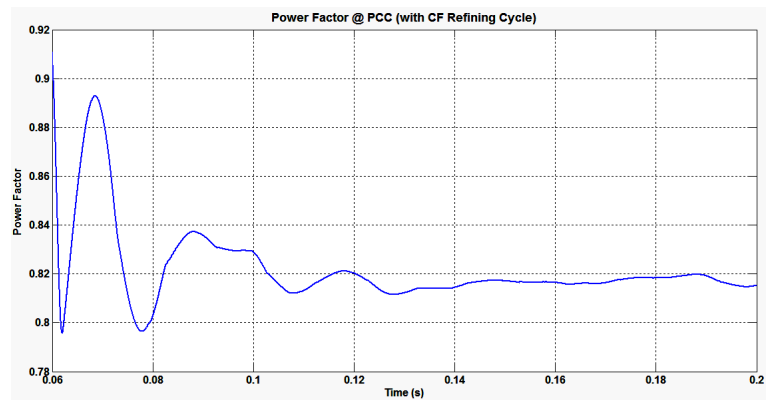
(f)



(g)



(h)



(i)

**Figure 5.4 Filter performance in EAF refining cycle (a) VIC without filter (b) PQS powers without filter (c) power factor without filter (d) VIC with PF (e) PQS powers with PF (f) power factor with PF (g) VIC with CF (h) PQS powers with CF (i) power factor with CF**

Figure 5.4 (c)-(f)-(i) shows power factor variation without filter, with PF and with CF application respectively at PCC. Table 5.2 shows tabulated values of active-reactive-apparent power and power factor after PF and CF application.

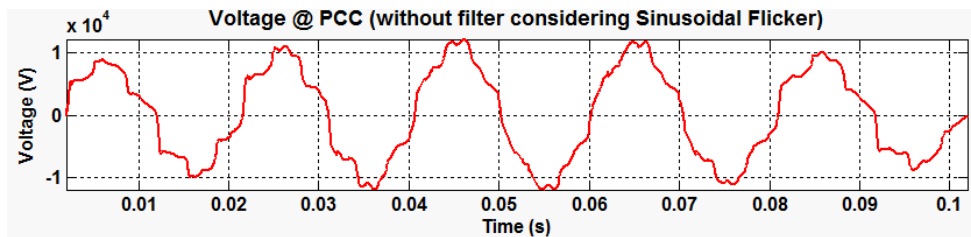
It can be seen from Table 5.2 that the power factor without filter is 0.59 which is improved to 0.56 and then to 0.82 after PF and CF application respectively in refining cycle of the EAF distribution network at PCC. It means CF performs better than PF alone in power factor improvement.

**Table 5.2 Power analysis in refining cycle**

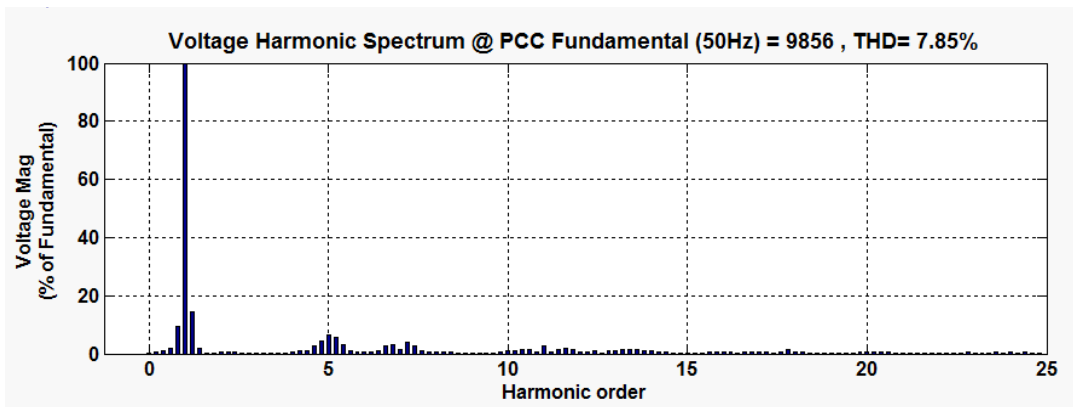
Parameters/condition	Phase	P (kW)	Q (kVAr)	S (kVA)	pf
Without filter	Phase-a	7131	2682	7627	0.59
	Phase-b	7054	2642	7541	0.59
	Phase-c	7106	2693	7607	0.59
With PF	Phase-a	8602	2056	8844	0.56
	Phase-b	8595	2060	8839	0.56
	Phase-c	8588	2063	8833	0.56
With CF	Phase-a	5227	6945	8701	0.82
	Phase-b	5718	7195	9238	0.81
	Phase-c	5263	7416	9183	0.82

**5.2.2 Performance analysis of CF in melting cycle (sinusoidal flicker)**

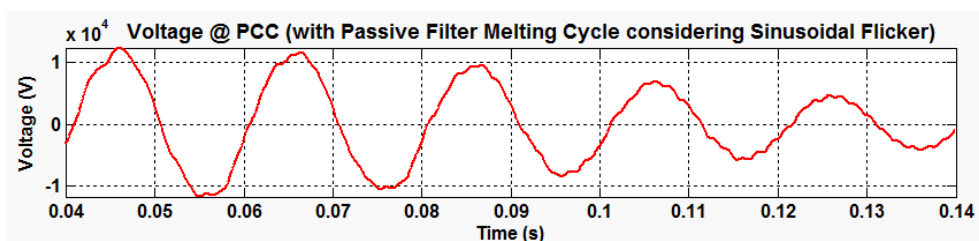
Figure 5.5 shows filter performance in melting cycle considering sinusoidal flicker of the EAF connected distribution network. Figure 5.5 (a)-(c)-(e) shows  $V_{PCC}$  waveforms without filter, with PF and with CF respectively. Figure 5.2 (b)-(d)-(f) shows harmonic spectrum of  $V_{PCC}$  without filter, with PF and with CF respectively.



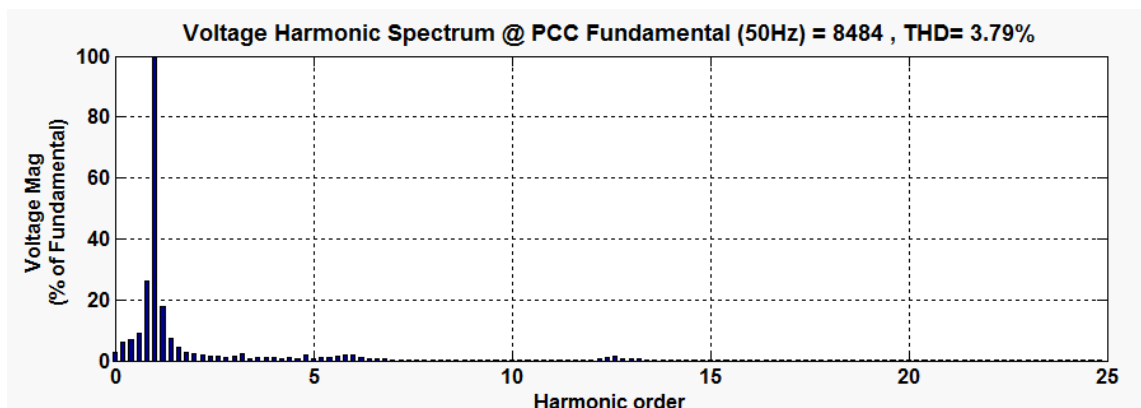
(a)



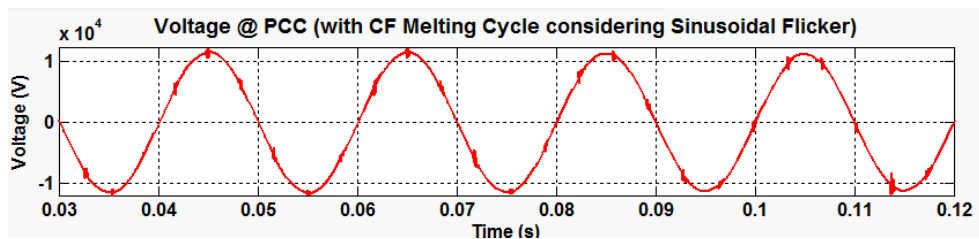
(b)



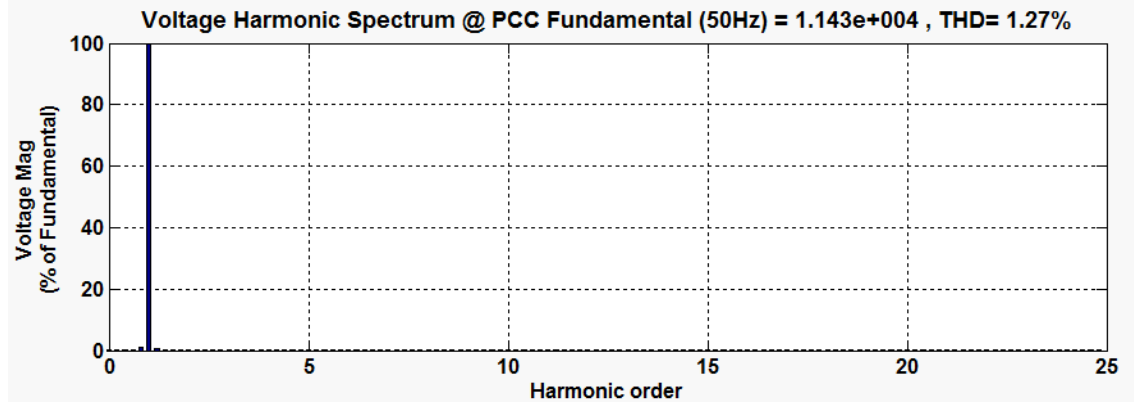
(c)



(d)



(e)



(f)

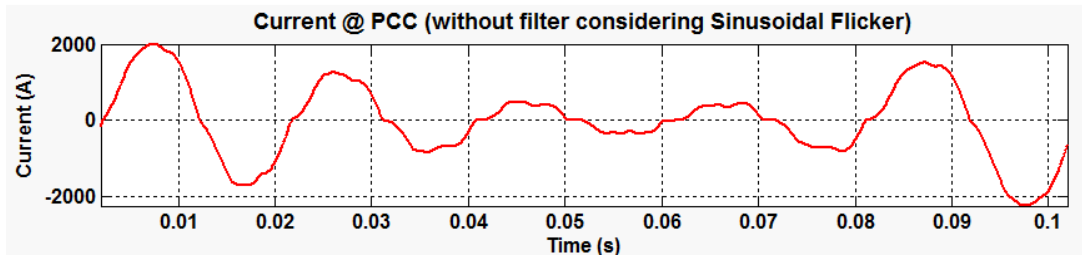
**Figure 5.5 Filter performance in EAF melting cycle (sinusoidal flicker) (a)  $V_{PCC}$  without filter (b) harmonic spectrum without filter (c)  $V_{PCC}$  with PF (d) harmonic spectrum with PF (e)  $V_{PCC}$  with CF (f) harmonic spectrum with CF**

The total harmonic distortion of voltage ( $THD_V$ ) observed at PCC is 7.85 % without filter in melting cycle considering sinusoidal flicker of EAF connected distribution network as shown in Figure 5.2 (b). This value is violating IEEE 519-1992 limits. It should be below 5%. That is improved to 3.79 % after passive filter application as shown in Figure 5.2 (d), which is within the IEEE 519-1992. An application of series APF along with passive filter changes  $THD_V$  to 1.27 % as shown in Figure 5.2 (f). That means CF performs better than the PF in improving  $THD_V$  in melting cycle considering sinusoidal flicker of EAF connected distribution network.

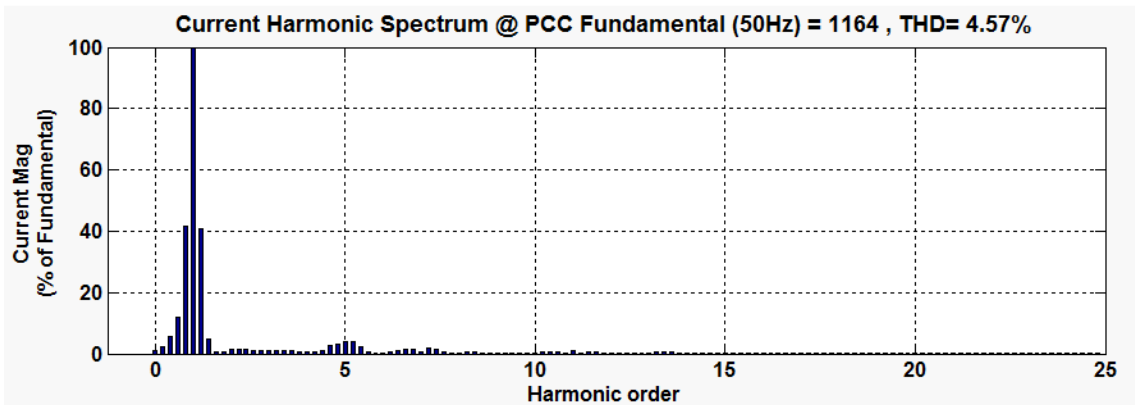
Table 5.3 show three phase harmonic spectrum details of voltage and current at PCC respectively for melting cycle considering sinusoidal flicker of the EAF connected distribution network. It can be seen that 5<sup>th</sup>, 7<sup>th</sup>, 11<sup>th</sup> and 13<sup>th</sup> are the major harmonic components present in voltage at PCC.  $H_5$  is more than IEEE 519-1992 limit of 5 % of harmonic distortion. It can be seen from Table 5.2 that both PF and CF can suppress individual harmonic components within the limit in melting cycle (sinusoidal flicker) of EAF distribution network at PCC but CF performs better than the PF.

Figure 5.6 shows filter performance in melting cycle considering sinusoidal flicker of the EAF connected network. Figure 5.3 (a)-(c)-(e) shows  $I_{PCC}$  waveforms without filter, with

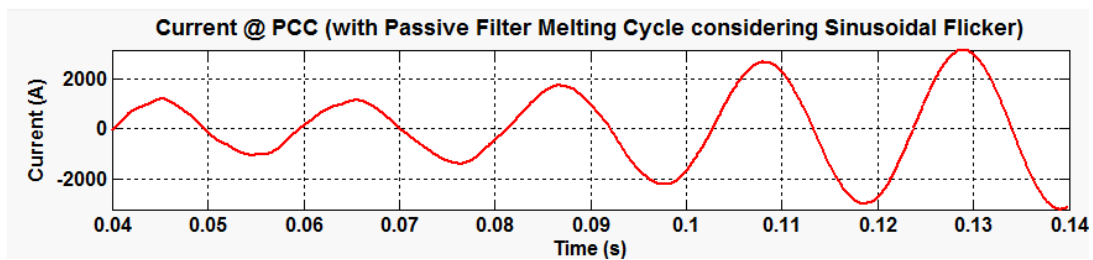
PF and with CF respectively. Figure 5.3 (b)-(d)-(f) shows harmonic spectrum of  $I_{PCC}$  without filter, with PF and with CF respectively.



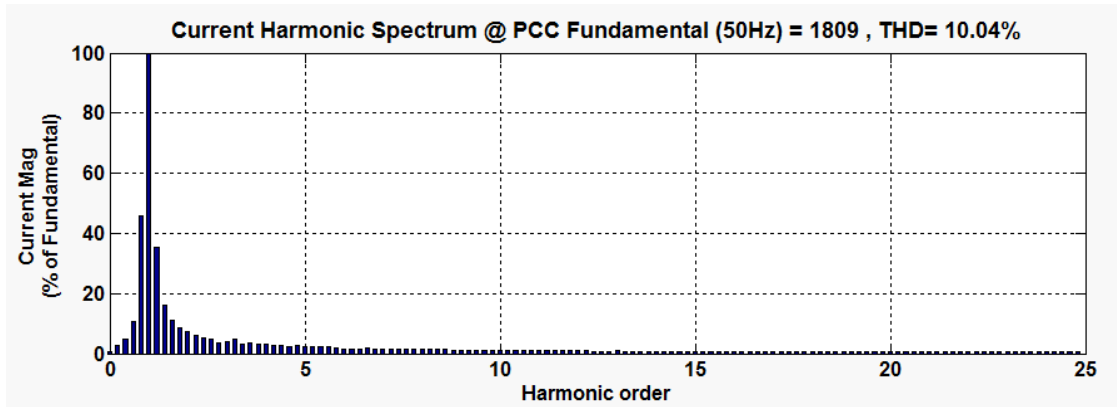
(a)



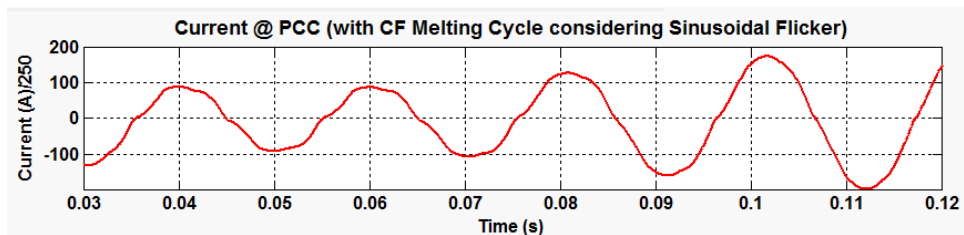
(b)



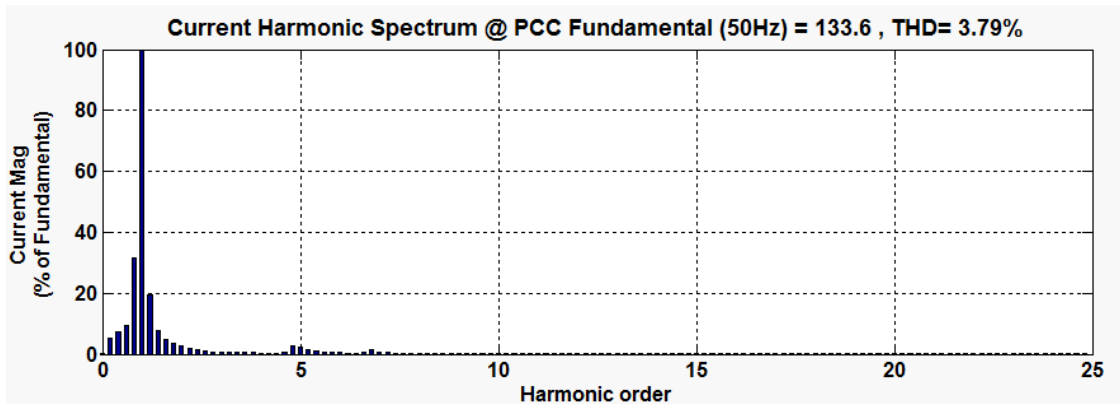
(c)



(d)



(e)



(f)

**Figure 5.6 Filter performance in EAF melting cycle considering random flicker (a)  $I_{PCC}$  without filter (b) harmonic spectrum without filter (c)  $I_{PCC}$  with PF (d) harmonic spectrum with PF (e)  $I_{PCC}$  with CF (f) harmonic spectrum with CF**

The total harmonic distortion of current ( $THD_I$ ) observed at PCC is 4.57 % without filter in refining cycle of EAF connected distribution network as shown in Figure 5.3 (b). It has changed to 10.04 % after PF application as shown in Figure 5.6 (d), which is violating

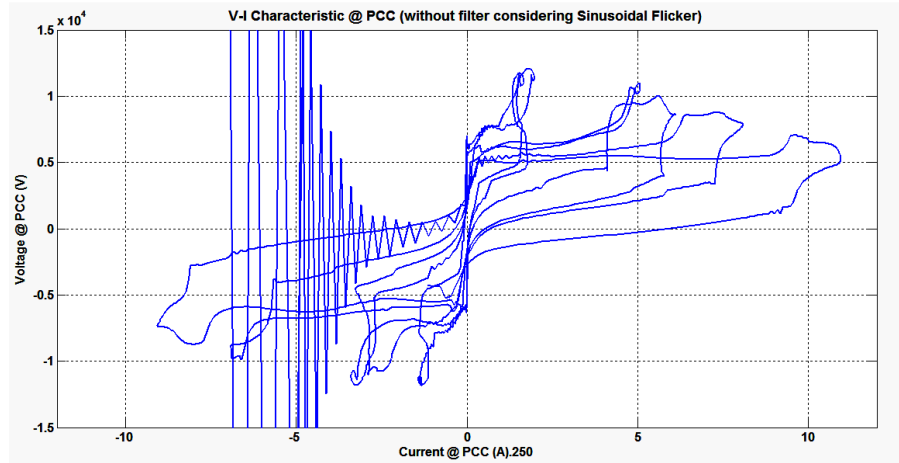
IEEE 519-1992. That means PF is detuned and its performance has deteriorated for melting cycle considering sinusoidal flicker of the EAF operation. Application of CF changes to 3.79 % as shown in Figure 5.6 (f), which are within the permissible limits.

**Table 5.3 Harmonic analysis of EAF connected distribution network in melting cycle (sinusoidal flicker)**

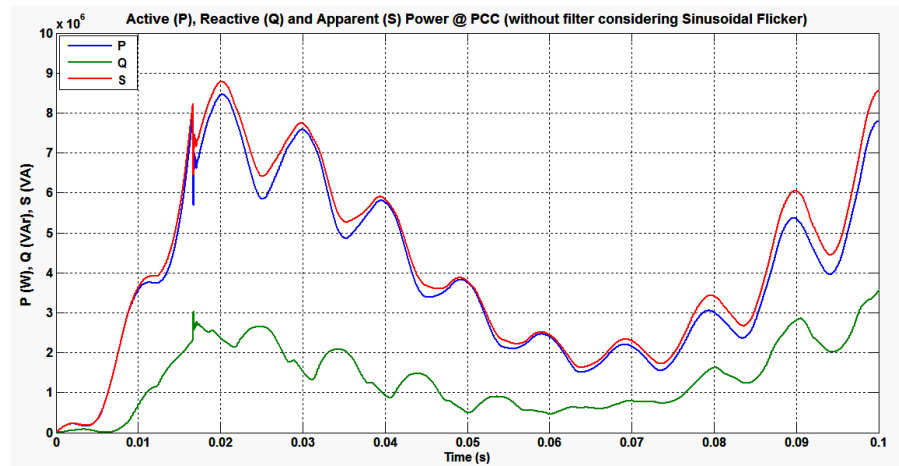
Parameters/condition	Phase	V/I	THD (%)	RMS	Fund.	H <sub>5</sub> (%)	H <sub>7</sub> (%)	H <sub>11</sub> (%)	H <sub>13</sub> (%)
Without filter	Phase-a	V	7.85	6970	9856	6.63	1.63	2.83	0
		I	4.57	823.2	1164	3.95	0	0	0
	Phase-b	V	8.29	6937	9811	6.83	1.56	3.13	1.1
		I	6.62	787.7	1114	4.91	1.17	0	0
	Phase-c	V	8.65	6956	9838	7.03	1.89	2.74	1.02
		I	6.98	817.9	1157	3.74	0	0	0
With PF	Phase-a	V	3.79	5999	8484	0.76	0.19	0.1	0
		I	10.04	1279	1809	2.36	0	0	0
	Phase-b	V	5.5	6150	8697	0.86	0.63	0.48	0
		I	7.43	1280	1810	1.55	0	0	0
	Phase-c	V	6.32	5997	8482	1.11	0.83	0.57	0.76
		I	5.48	1236	1748	0.96	0	0	0
With CF	Phase-a	V	1.27	8084	11430	0.39	0.14	0.07	0.04
		I	5.02	96.78	136.9	2.32	0.25	0.41	0.39
	Phase-b	V	1.36	8090	11440	0.34	0.11	0.09	0.07
		I	4.36	96.61	136.6	1.42	0.68	0.56	0.35
	Phase-c	V	1.35	8089	11440	0.38	0.13	0.09	0.08
		I	3.79	94.49	133.6	2.37	0.53	0.21	0.2

Harmonics spectrum quantified detail is tabulated in Table 5.2. That means PF performs better than CF in reducing THD<sub>I</sub> in melting cycle (sinusoidal flicker).

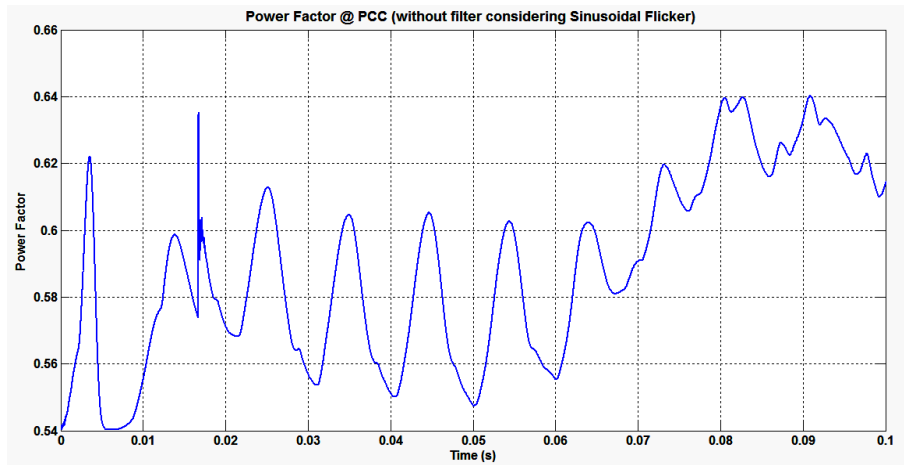
Figure 5.7 (a)-(c)-(e) depicts typical VICs without filter, with PF and with CF application respectively. Figure 5.4 (b)-(d)-(f) shows active-reactive power consumption at PCC by the EAF without filter, with PF and with CF application respectively.



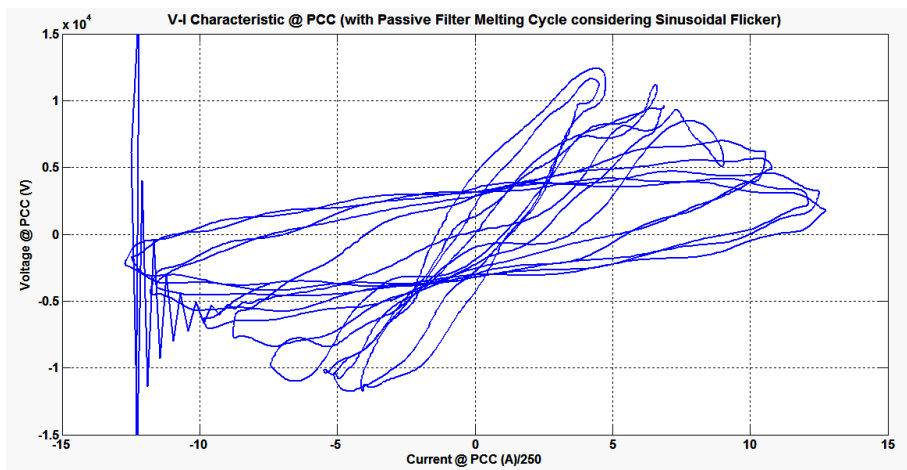
(a)



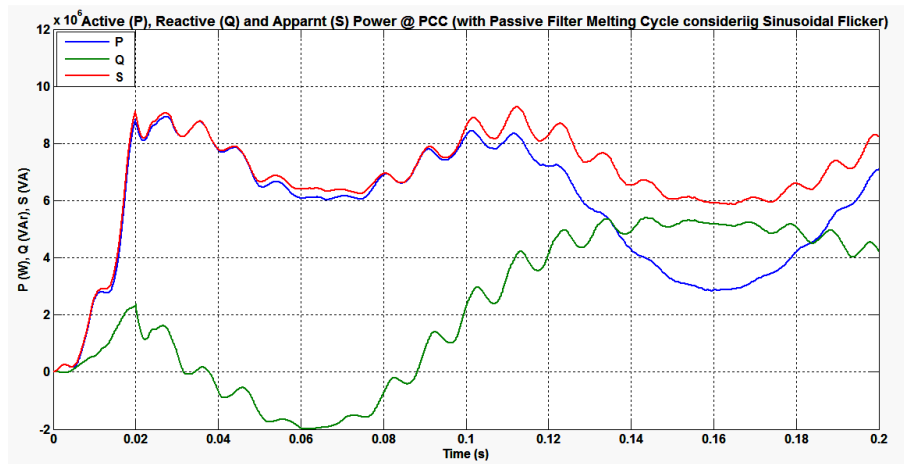
(b)



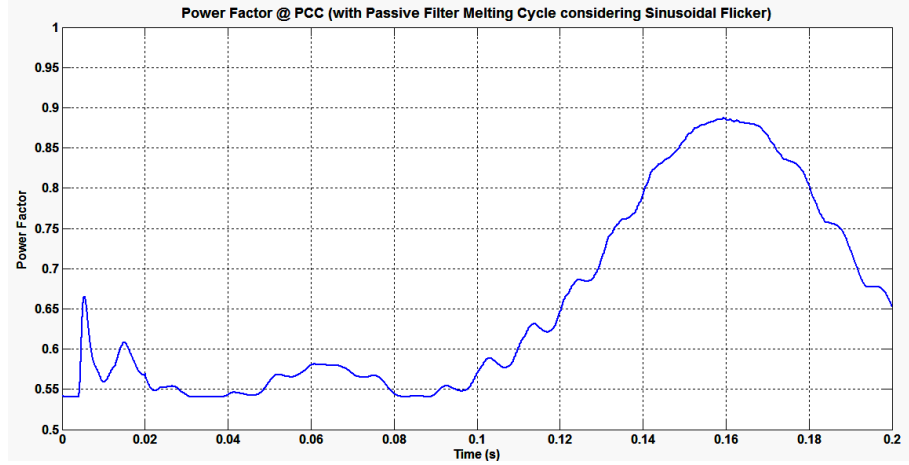
(c)



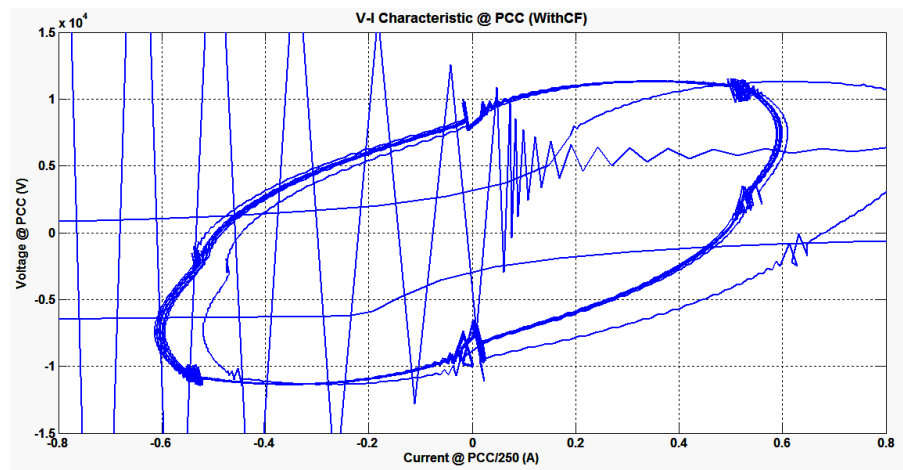
(d)



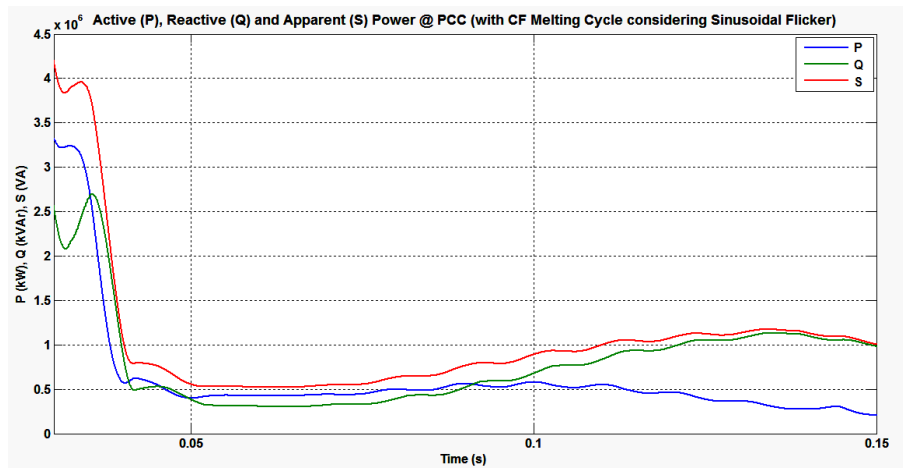
(e)



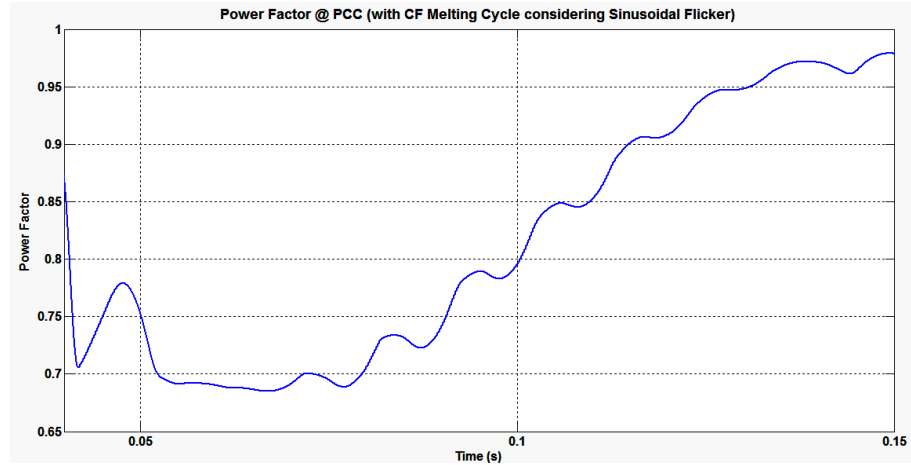
(f)



(g)



(h)



(i)

**Figure 5.7 Filter performance in EAF melting cycle considering sinusoidal flicker (a) VIC without filter (b) PQS powers without filter (c) power factor without filter (d) VIC with PF (e) PQS powers with PF (f) power factor with PF (g) VIC with CF (h) PQS powers with CF (i) power factor with CF**

Figure 5.7 (c)-(f)-(i) shows power factor variation without filter, with PF and with CF application respectively at PCC. Table 5.4 shows tabulated values of active-reactive-apparent power and power factor after PF and CF application.

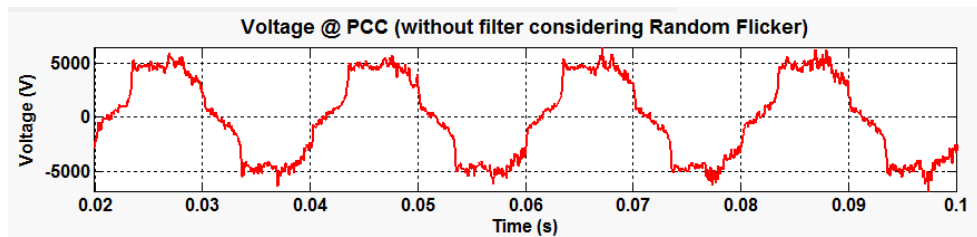
**Table 5.4 Power analysis in melting cycle (sinusoidal flicker)**

Parameters/condition	Phase	P (kW)	Q (kVAr)	S (kVA)	pf
Without filter	Phase-a	4771	2485	5448	0.62
	Phase-b	4772	2495	5454	0.62
	Phase-c	4769	2495	5452	0.62
With PF	Phase-a	6862	1138	7433	0.59
	Phase-b	6955	1092	7531	0.59
	Phase-c	6904	1193	7472	0.59
With CF	Phase-a	6658	1020	7435	0.86
	Phase-b	8193	1145	7471	0.86
	Phase-c	7209	1137	8489	0.86

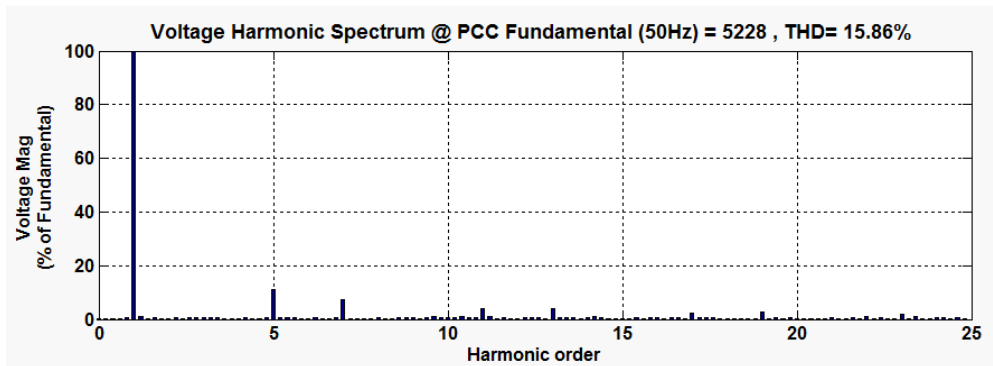
It can be seen from Table 5.4 that the power factor without filter is 0.59 which is improved to 0.62 and later to 0.86 after PF and CF application respectively in melting cycle (sinusoidal flicker) of the EAF distribution network at PCC. It means CF performs better than PF alone in power factor improvement.

### 5.2.3 Performance analysis of CF in melting cycle (random flicker)

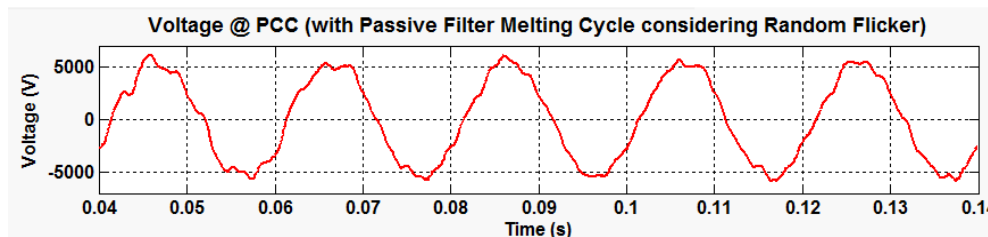
Figure 5.8 shows filter performance in melting cycle considering random flicker of the EAF connected distribution network. Figure 5.8 (a)-(c)-(e) shows  $V_{PCC}$  waveforms without filter, with PF and with CF respectively. Figure 5.8 (b)-(d)-(f) shows harmonic spectrum of  $V_{PCC}$  without filter, with PF and with CF respectively.



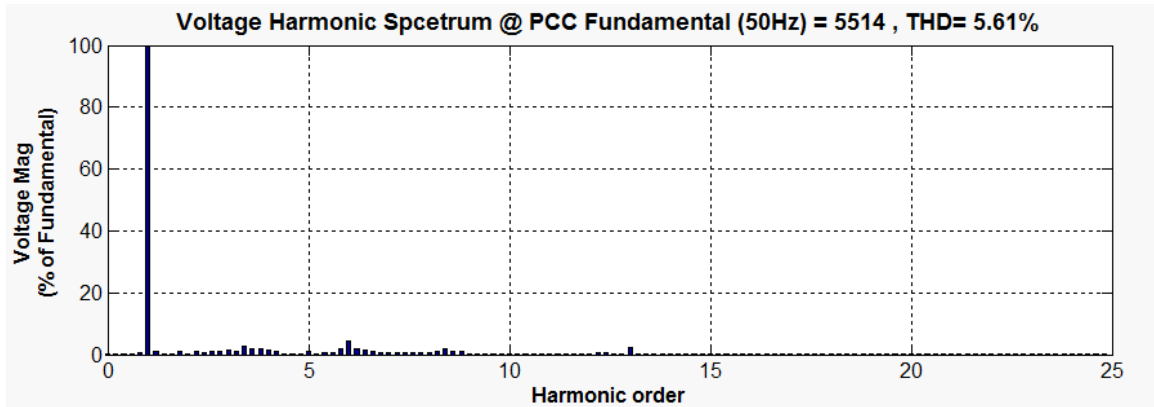
(a)



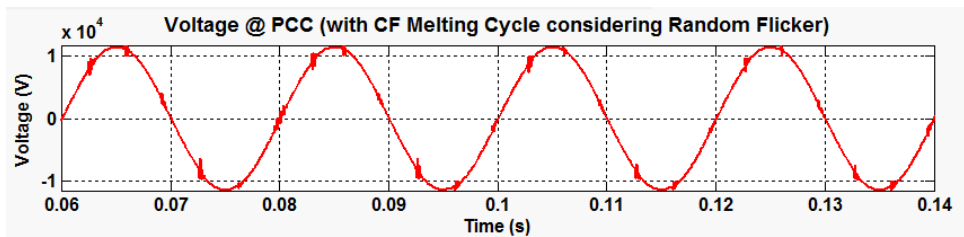
(b)



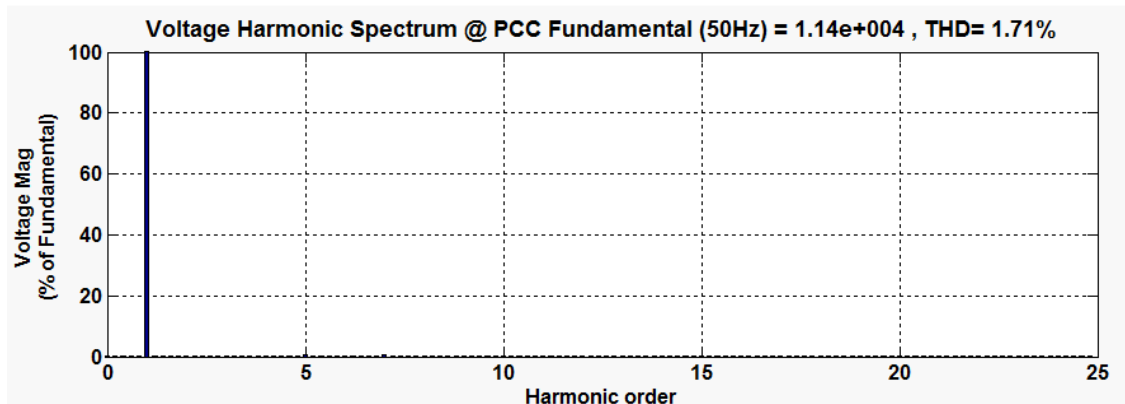
(c)



(d)



(e)



(f)

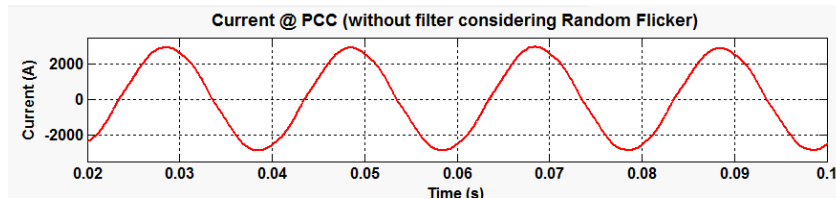
**Figure 5.8 Filter performance in EAF melting cycle (random flicker) (a)  $V_{PCC}$  without filter (b) harmonic spectrum without filter (c)  $V_{PCC}$  with PF (d) harmonic spectrum with PF (e)  $V_{PCC}$  with CF (f) harmonic spectrum with CF**

The total harmonic distortion of voltage ( $THD_V$ ) observed at PCC is 15.86 % without filter in melting cycle considering random flicker of EAF connected distribution network as shown in Figure 5.8 (b). This value is violating IEEE 519-1992 limits. It should be below

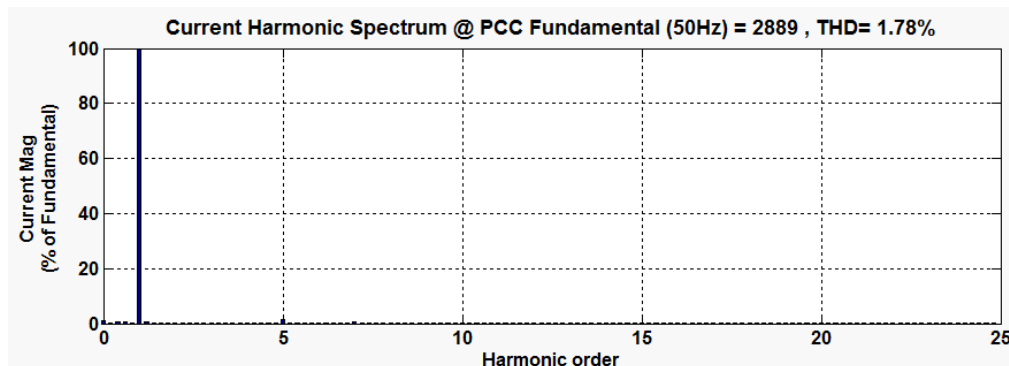
5%. That is improved to 5.61 % after passive filter application as shown in Figure 5.8 (d), which is nearer to the IEEE 519-1992 limit of 5 % but little more than the required. An application of CF changes THD<sub>v</sub> to 1.71 % as shown in Figure 5.8 (f). That means CF performs better than PF in improving THD<sub>v</sub> in melting cycle considering sinusoidal flicker of EAF connected distribution network.

Table 5.5 show three phase harmonic spectrum details of voltage and current at PCC for melting cycle considering random flicker of the EAF connected distribution network.. It can be seen that 5<sup>th</sup>, 7<sup>th</sup>, 11<sup>th</sup> and 13<sup>th</sup> are the major harmonic components present in voltage at PCC and are more than IEEE 519-1992 limit of 5 % of harmonic distortion. It can be seen from Table 5.5 that both PF and CF can suppress individual harmonic components within the limit in refining cycle of EAF distribution network at PCC but CF performs better than the PF.

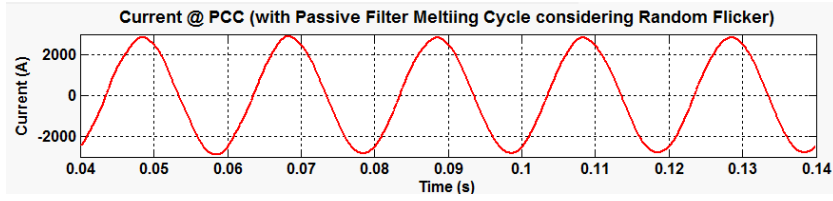
Figure 5.9 shows filter performance in melting cycle considering random flicker of the EAF connected network. Figure 5.9 (a)-(c)-(e) shows I<sub>PCC</sub> waveforms without filter, with PF and with CF respectively. Figure 5.9 (b)-(d)-(f) shows harmonic spectrum of I<sub>PCC</sub> without filter, with PF and with CF respectively.



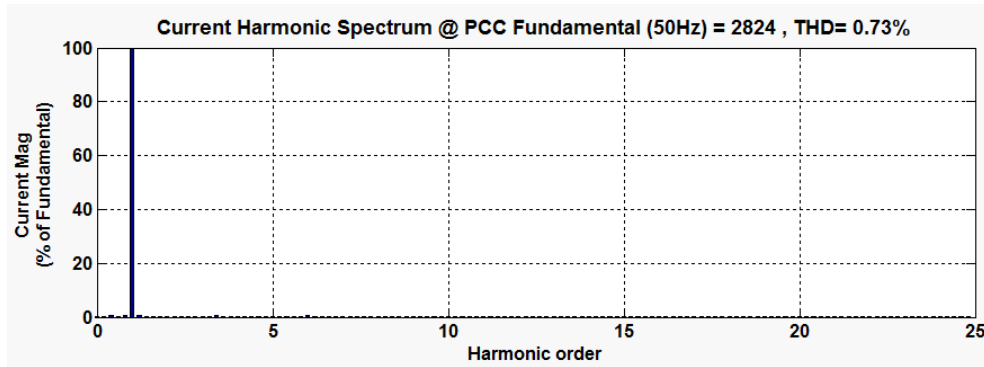
(a)



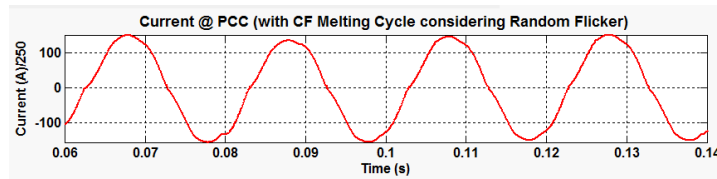
(b)



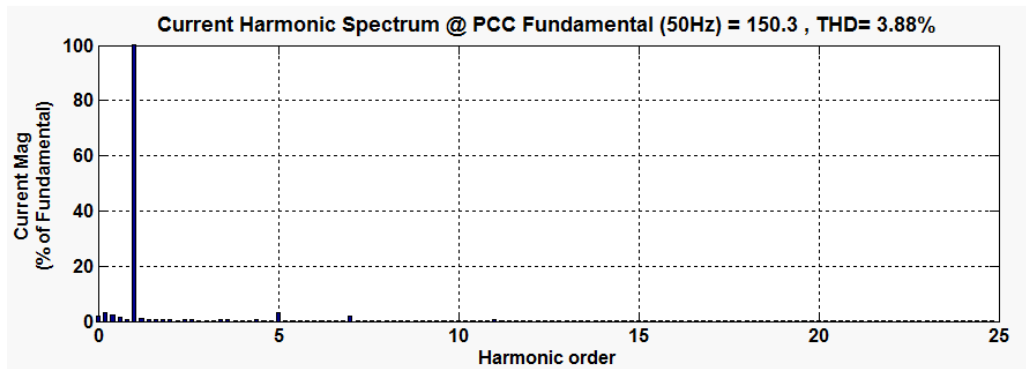
(c)



(d)



(e)



(f)

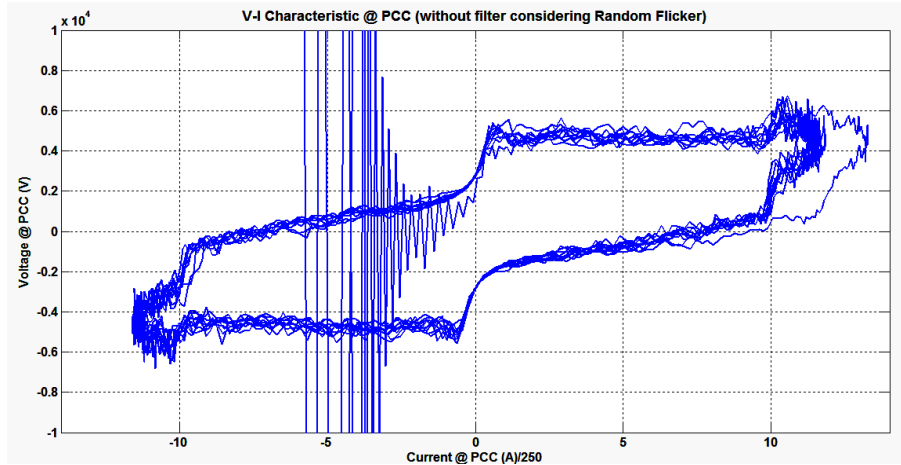
Figure 5.9 Filter performance in EAF melting cycle considering random flicker (a)  $I_{PCC}$  without filter (b) harmonic spectrum without filter (c)  $I_{PCC}$  with PF (d) harmonic spectrum with PF (e)  $I_{PCC}$  with CF (f) harmonic spectrum with CF

The total harmonic distortion of current (THD<sub>i</sub>) observed at PCC is 1.78 % without filter in refining cycle of EAF connected distribution network as shown in Figure 5.9 (b), which is within the IEEE 519-1992 limit of 5%. It has changed to 0.73 and then to 3.88 % after PF and CF application as shown in Figure 5.9 (d) and Figure 5.9 (f) respectively. Harmonics spectrum quantified detail is tabulated in Table 5.5.

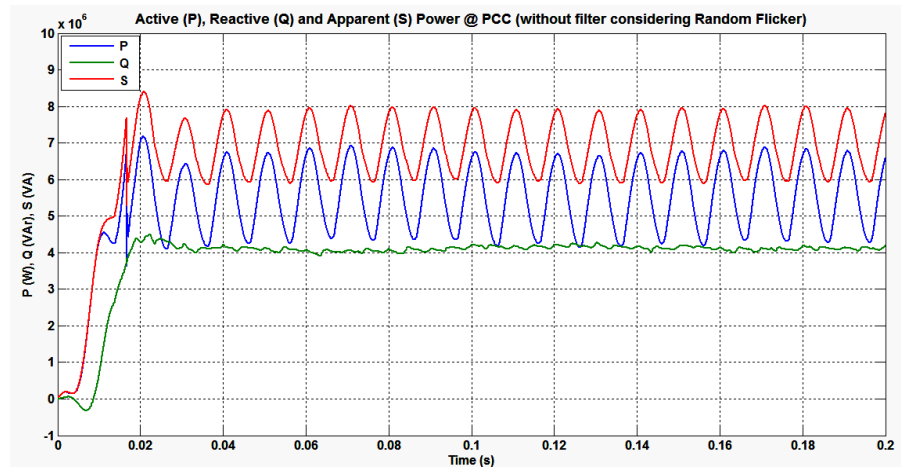
**Table 5.5 Harmonic analysis of EAF connected distribution network in melting cycle (random flicker)**

Parameters/condition	Phase	V/I	THD (%)	RMS	Fund.	H <sub>5</sub> (%)	H <sub>7</sub> (%)	H <sub>11</sub> (%)	H <sub>13</sub> (%)
Without filter	Phase-a	V	15.86	3697	5228	11	7.48	4.06	4.1
		I	1.78	2043	2889	1.51	0	0	0
	Phase-b	V	15.98	3687	5214	11.29	7.62	4.21	3.32
		I	1.82	2035	2878	1.58	0	0	0
	Phase-c	V	15.63	3706	5241	10.69	7.86	4.05	0
		I	1.77	2028	2868	1.43	0	0	0
With PF	Phase-a	V	5.61	3899	5514	0.89	0.67	0.03	2.33
		I	0.73	1997	2824	0.12	0	0	0
	Phase-b	V	4.65	3886	5496	1.12	0.22	0.12	1.99
		I	0.72	1997	2824	0.15	0	0	0
	Phase-c	V	3.45	3903	5519	0.97	0.45	0.1	1.7
		I	0.64	1992	2818	0.05	0	0	0
With CF	Phase-a	V	1.71	8064	1140	0.65	0.42	0.22	0.19
		I	3.88	16.3	150.4	3.32	1.69	0.53	0.3
	Phase-b	V	1.92	8067	11410	0.68	0.43	0.25	0.15
		I	4.32	105.3	149.6	3.72	1.73	0.6	0.36
	Phase-c	V	1.92	8068	1140	0.66	0.42	0.25	0.14
		I	4.27	106.1	149.7	3.5	1.74	0.68	0.28

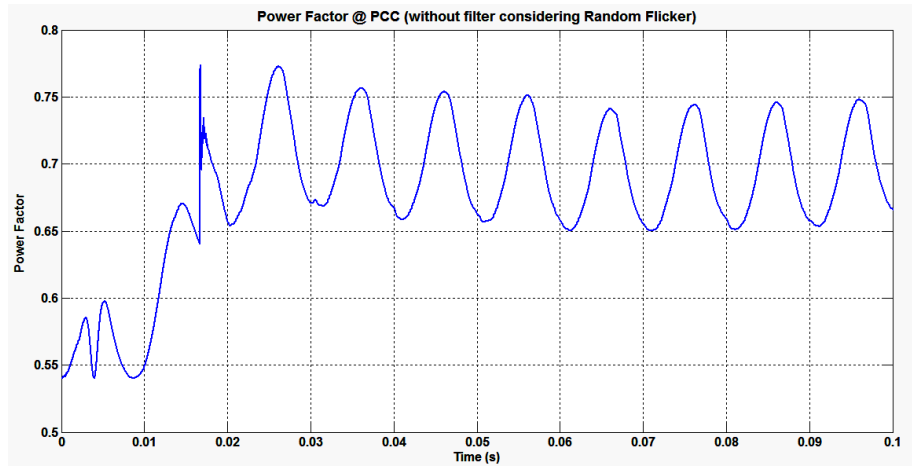
Figure 5.10 (a)-(c)-(e) depicts typical VICs without filter, with PF and with CF application respectively. Figure 5.10 (b)-(d)-(f) shows active-reactive power consumption at PCC by the EAF without filter, with PF and with CF application respectively.



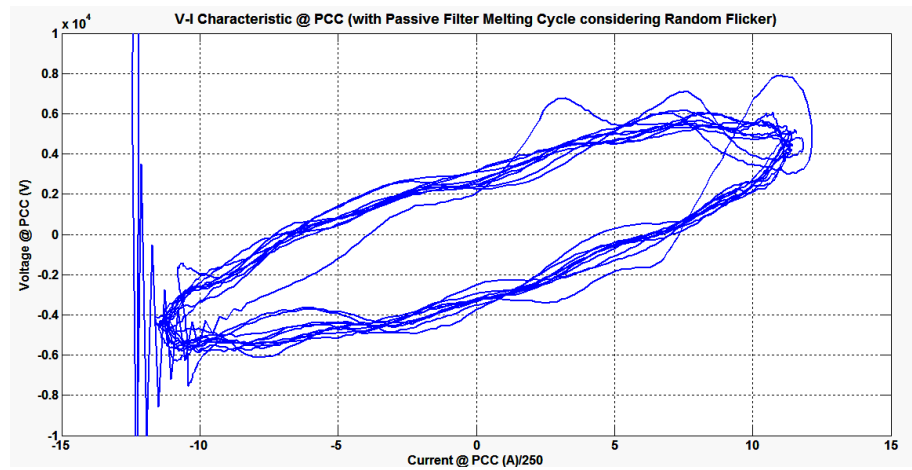
(a)



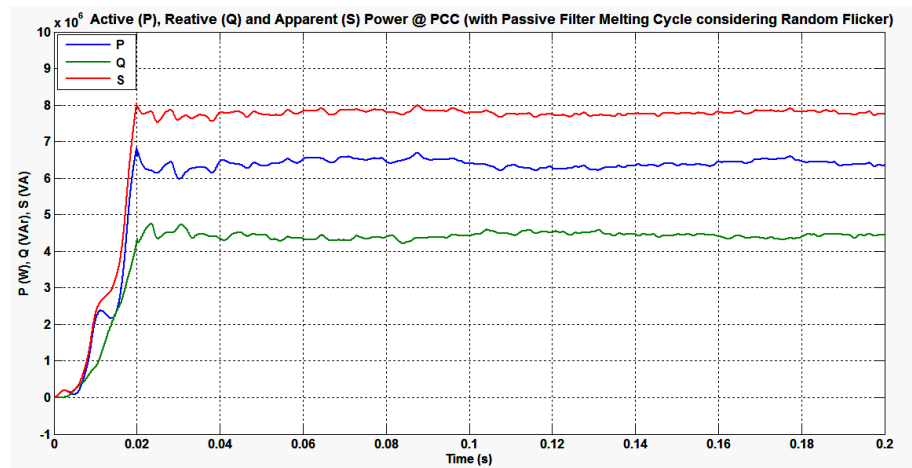
(b)



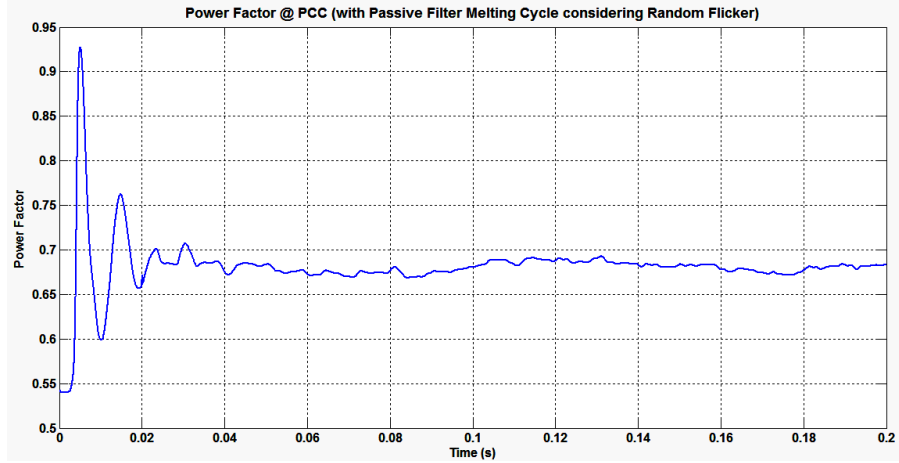
(c)



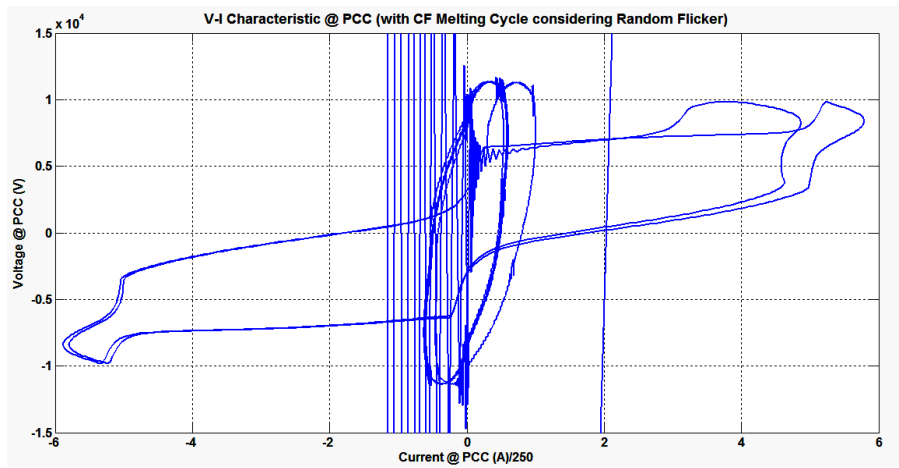
(d)



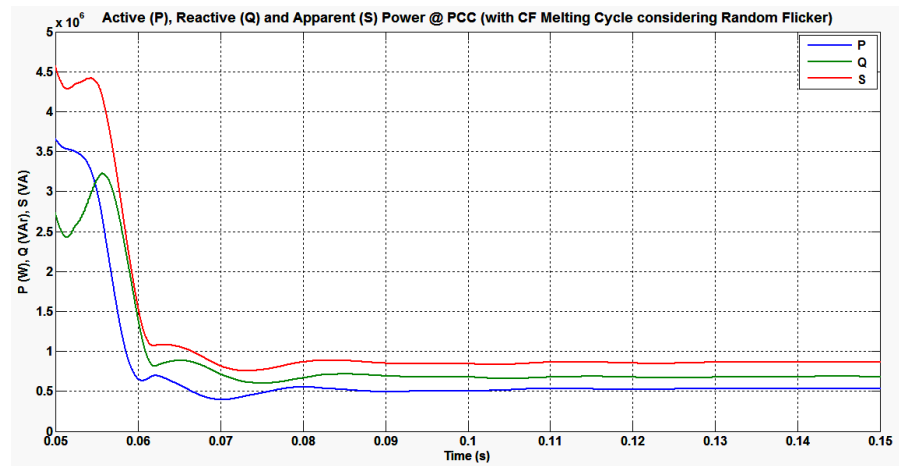
(e)



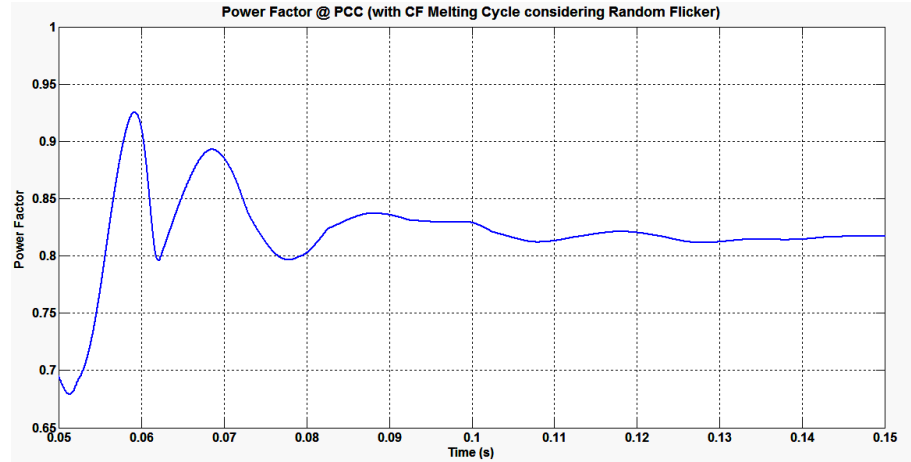
(f)



(g)



(h)



(i)

**Figure 5.10 Filter performance in EAF melting cycle considering random flicker (a) VIC without filter (b) PQS powers without filter (c) power factor without filter (d) VIC with PF (e) PQS powers with PF (f) power factor with PF (g) VIC with CF (h) PQS powers with CF (i) power factor with CF**

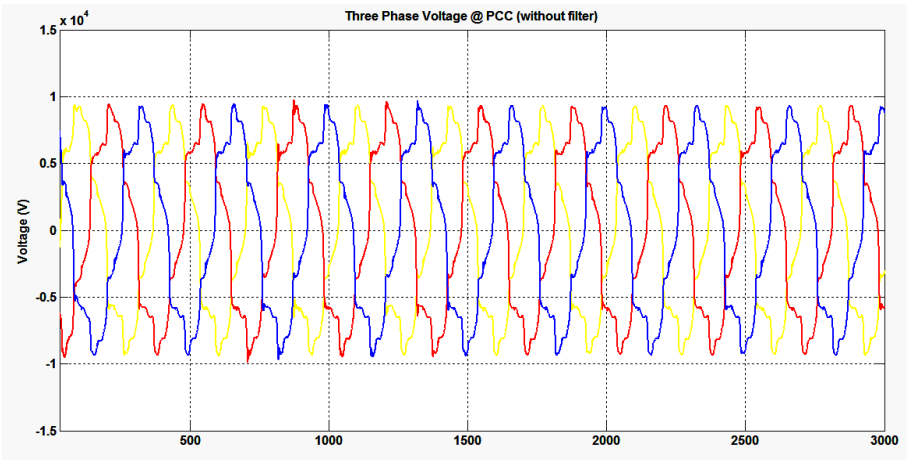
Figure 5.10 (c)-(f)-(i) shows power factor variation without filter, with PF and with CF application respectively at PCC. Table 5.6 shows tabulated values of active-reactive-apparent power and power factor after PF and CF application.

**Table 5.6 Power analysis in melting cycle (random flicker)**

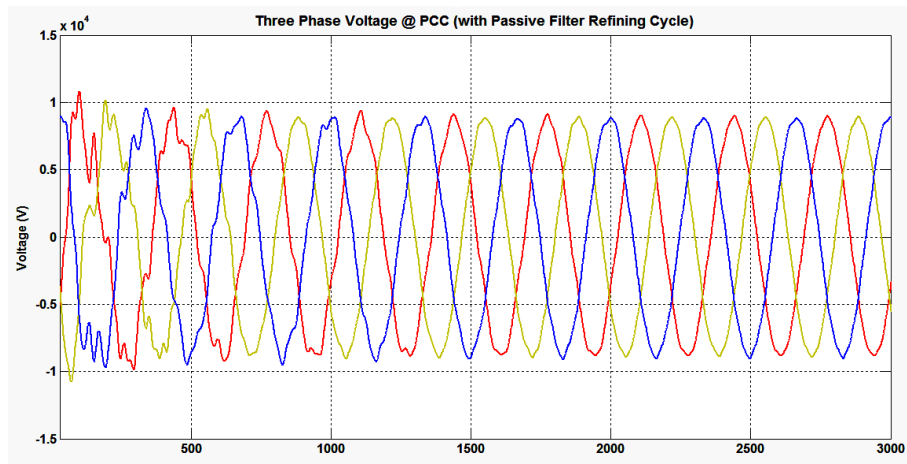
Parameters/condition	Phase	P (kW)	Q (kVAr)	S (kVA)	pf
Without filter	Phase-a	6028	4552	7554	0.69
	Phase-b	6000	4560	7536	0.69
	Phase-c	6013	4561	7547	0.69
With PF	Phase-a	6406	4424	7786	0.68
	Phase-b	6342	4454	7752	0.68
	Phase-c	6371	4453	7774	0.68
With CF	Phase-a	5227	6945	8701	0.82
	Phase-b	5718	7195	9238	0.81
	Phase-c	5263	7416	9183	0.82

It can be seen from Table 5.6 that the power factor without filter is 0.68 which is improved to 0.69 and later to 0.82 after PF and CF application respectively in melting cycle (random flicker) of the EAF distribution network at PCC. It means CF performs better than PF alone in power factor improvement.

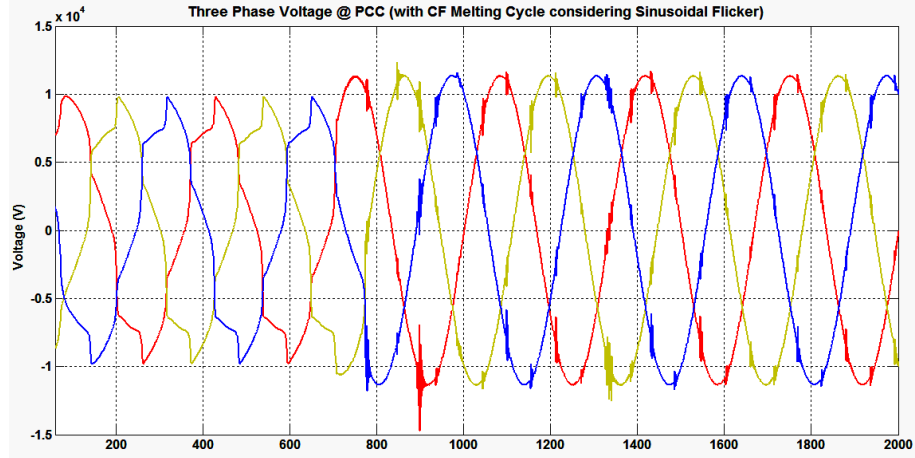
Figure 5.11 shows three phase voltages at PCC under refining cycle condition of EAF connected distribution network.



(a)



(b)

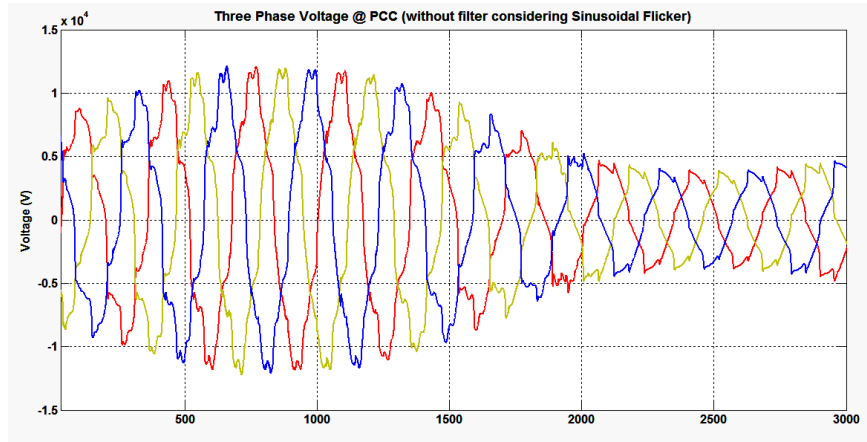


(c)

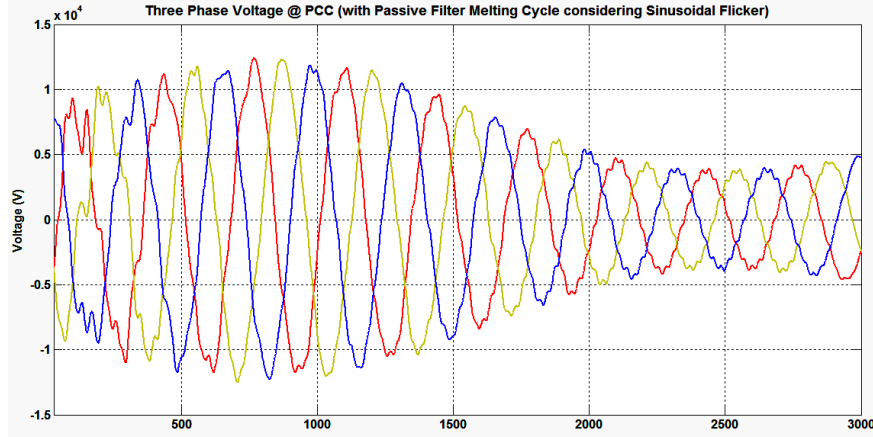
**Figure 5.11 Three phase  $V_{PCC}$  for refining cycle (a) without filter (b) with PF (c) with CF**

Figure 5.11 (a)-(b)-(c) shows three-phase  $V_{PCC}$  without filter, with PF and with CF application respectively at PCC.

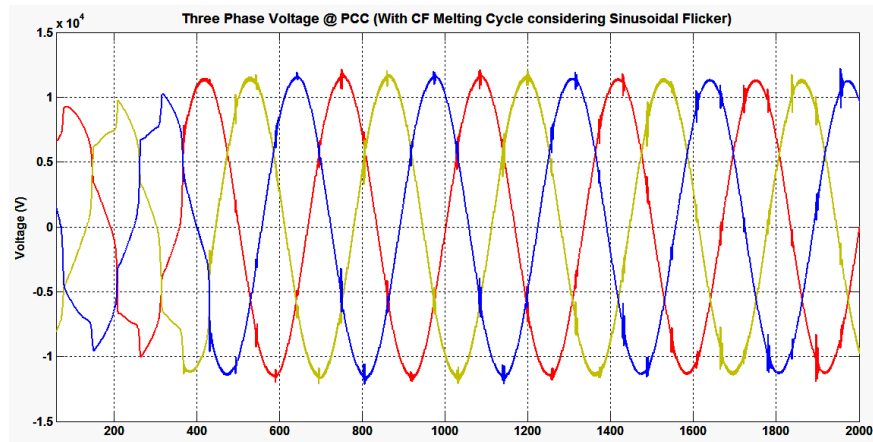
Figure 5.12 (a)-(b)-(c) shows three-phase  $V_{PCC}$  without filter, with PF and with CF application respectively at PCC under melting cycle considering sinusoidal flicker of EAF connected distribution network.



(a)



(b)



(c)

**Figure 5.12 Three phase  $V_{PCC}$  for sinusoidal flicker (a) without filter (b) with PF (c) with CF**

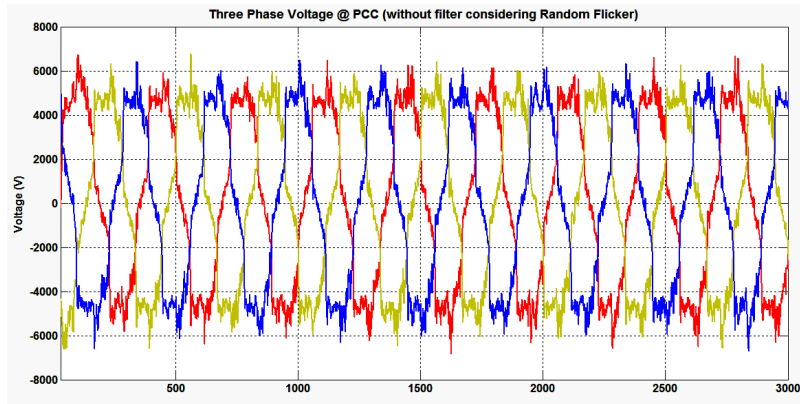
Comparison of Figure 5.12 (b) and Figure 5.11 (c) itself concludes better performance of CF than PF in removing sinusoidal flicker.

% Voltage flicker for sinusoidal variation is estimated using equation (2.16) for passive filter and composite filter application as shown in Table 5.7. Tabulated results and Figure 5.4 clearly show that the passive filter fails to clear sinusoidal voltage flicker whereas composite filter reduces voltage flicker from 2.92 % to 1.78 %. For 4 Hz of frequency pulsation applied and for 1.29 of % voltage pulsation (% voltage flicker) with composite filter, the operating point lies in non-perceptible zone as per the Fig. 5. Which means composite filter brings voltage flicker in within non-perceptible criteria.

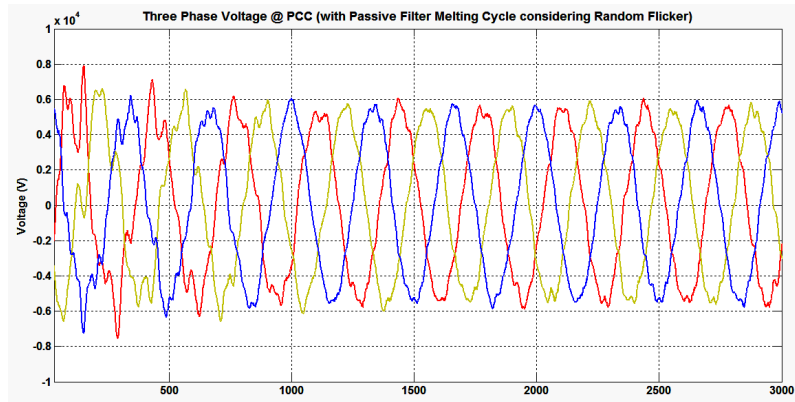
**Table 5.7 Voltage flicker analysis**

Parameters	Without Filter	With PF	With CF
Voltage Measurement			
$V_{1P}$ (V)	5343	5621	3243
$V_{2P}$ (V)	10900	11490	11590
% Flicker Calculation			
% Voltage Flicker	2.92	2.92	1.78

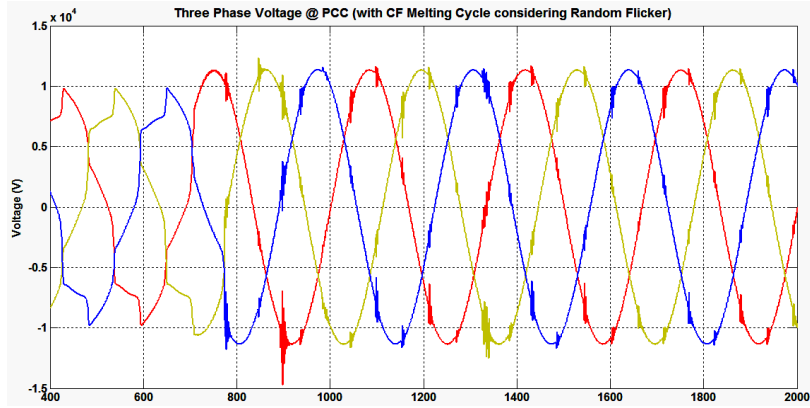
Figure 5.13 (a)-(b)-(c) shows three-phase  $V_{PCC}$  without filter, with PF and with CF application respectively at PCC under melting cycle considering random flicker of EAF connected distribution network.



**(a)**



**(b)**



(c)

**Figure 5.13 Three phase  $V_{PCC}$  for random flicker (a) without filter (b) with PF (c) with CF**

Comparison of Figure 5.13 (b) and Figure 5.13 (c) itself concludes better performance of CF than PF in removing random flicker.

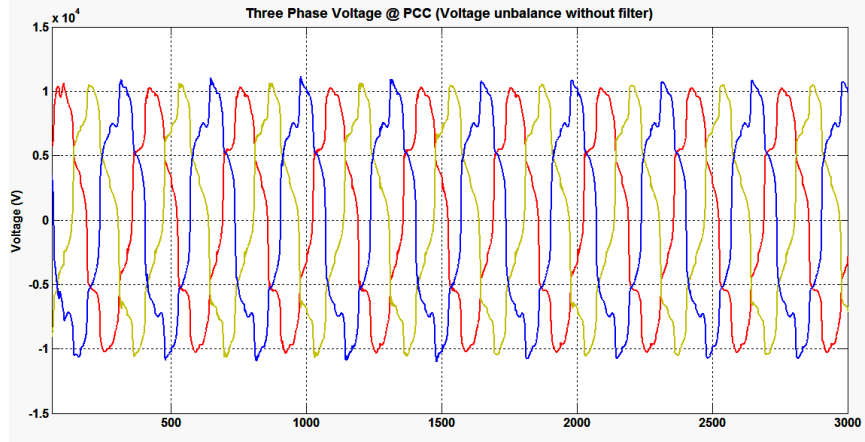
#### 5.2.4 Performance analysis of CF in voltage unbalance

Unbalance voltage condition is simulated by varying values of  $E_0$  in case of Cassie-Mayr's EAF model where as  $V_{at0}$  in case of the proposed EAF model as per Table 5.8.

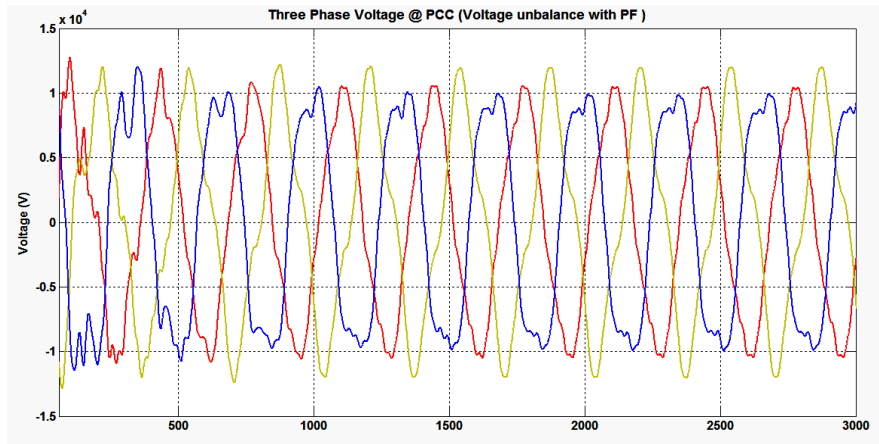
**Table 5.8 Voltage unbalances condition parameters**

Parameter	EAF Model 1 (Cassie-Mayr)	EAF Model 2 (Proposed)
$E_0=V_{at0}$ for a-Phase	250	250
$E_0=V_{at0}$ for b-Phase	300	300
$E_0=V_{at0}$ for c-Phase	350	350

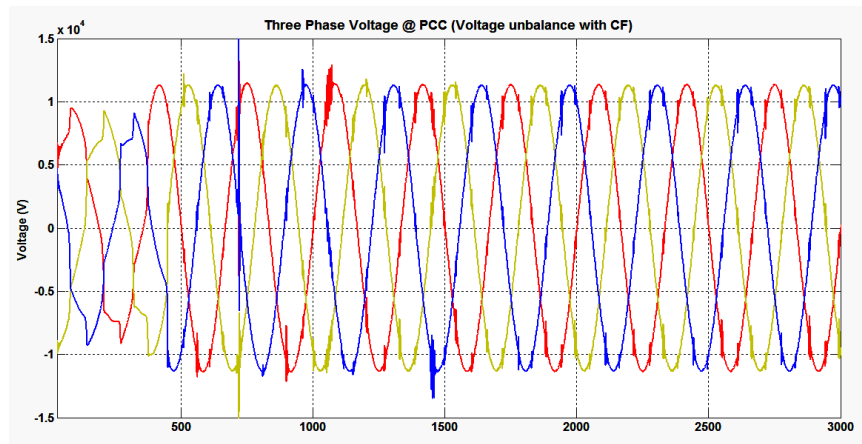
Simulated three phase voltage at PCC for voltage unbalance case has been shown in Figure 5.14.



(a)



(b)



(c)

Figure 5.14 Three phase voltage unbalance (a) without filter (b) with PF (c) with CF

The reflected phase voltage values both-peak and RMS are tabulated in Table 5.9.

**Table 5.9 Voltage unbalances analysis**

<b>Without Filter</b>				
<b>Parameter</b>	<b>Peak</b>	<b>RMS</b>	<b>Voltage Unbalance (Peak)</b>	<b>% Unbalance (Peak)</b>
Voltage Phase-a	9140	6463	106.30	6.31
Voltage Phase-b	8661	6124	100.73	0.73
Voltage Phase-c	7993	5652	92.96	-7.03
Voltage (Average)	8598.00	6079.67		
Voltage (Average Deviation)	403.33	285.11		
Voltage (% Average Deviation)	4.69	4.69		
<b>With Passive Filter</b>				
Voltage Phase-a	9632	6811	106.72	6.72
Voltage Phase-b	8946	6326	99.12	-0.88
Voltage Phase-c	8498	6009	94.16	-5.84
Voltage (Average)	9025.33	6382.00		
Voltage (Average Deviation)	404.44	286.00		
Voltage (% Average Deviation)	4.48	4.48		
<b>With Composite Filter</b>				
Voltage Phase-a	11420	8078	100.41	0.45
Voltage Phase-b	11350	8025	99.79	-0.21
Voltage Phase-c	11350	8022	99.79	-0.24
Voltage (Average)	11373	8041.7		
Voltage (Average Deviation)	31.11	24.22		
Voltage (% Average Deviation)	0.27	0.30		

From these values, average voltage deviation and per phase voltage deviation is calculated for peak and RMS values. It can be seen from Table 5.7 that the voltage unbalance has improved to 0.27 % from 4.69 % on an average.

### 5.3 Performance evaluation of CF

Performances of PF and CF for various operational cycles of EAF distribution network has been analyzed in this section. Table 5.10 shows percentage improvement in the respective voltage harmonic components after application of PF and CF. It can also be noted that performance of composite filter is better than the passive filter for H<sub>5</sub> and H<sub>7</sub> components, which are the major concern.

**Table 5.10 Filter performance in voltage harmonics reduction**

Parameter	Refining cycle		Melting cycle (Sinusoidal flicker)		Melting cycle (Random flicker)	
	With PF	With CF	With PF	With CF	With PF	With CF
H <sub>5</sub> (%)	94.77	94.64	86.68	94.58	90.96	93.97
H <sub>7</sub> (%)	95.87	94.75	65.72	92.52	94.16	94.47
H <sub>11</sub> (%)	98.74	96.79	86.78	97.13	97.97	94.16
H <sub>13</sub> (%)	65.96	94.16	64.15	91.04	18.87	93.53
THD <sub>v</sub> (%)	74.04	89.37	37.03	83.95	71.12	88.31

**Table 5.11 Filter performance in current harmonics reduction**

Parameter	Refining cycle		Melting cycle (Sinusoidal flicker)		Melting cycle (Random flicker)	
	With PF	With CF	With PF	With CF	With PF	With CF
H <sub>5</sub> (%)	96.82	47.77	61.35	51.51	92.92	94.9
H <sub>7</sub> (%)	98.21	57.68	100	24.79	100	100
H <sub>11</sub> (%)	100	78.28	100	100	100	100
H <sub>13</sub> (%)	100	64.84	100	100	100	100
THD <sub>i</sub> (%)	84.86	53.6	-26.31	27.52	61.08	88.18

Table 5.11 shows percentage improvement in the respective current harmonic components after application of PF and CF. It can also be noted that performance of CF is better than the PF for H5 and H7 components, which are the major concern.

Table 5.12 shows percentage improvement in the power factor at PCC after application of PF and CF. It can be seen that performance of CF is better than the PF.

**Table 5.12 Filter performance in power factor improvement**

Parameter	Refining cycle		Melting cycle (Sinusoidal flicker)		Melting cycle (Random flicker)	
	With PF	With CF	With PF	With CF	With PF	With CF
Power Factor	5.08	38.98	4.84	38.71	1.45	18.84

Table 5.13 shows performance of PF and CF under voltage unbalanced condition. Tabulated results show that PF alone fails to clear voltage unbalance whereas CF performs better than PF.

**Table 5.13 Filter performance in voltage unbalance clearance**

Parameter	Without filter	With PF	With CF
Peak voltage unbalance (%)	4.69	4.48	93.97
RMS voltage unbalance (%)	4.69	4.48	93.30

Voltage unbalance during arcing is the one of the important phenomenon in EAF. The designed CF has capability of clearing this voltage unbalance as per the tabulated results in Table 5.14, which again confirms better performance of CF in reducing voltage flicker than PF alone.

**Table 5.14 Filter performance in reducing voltage flicker**

Parameter	Without filter	With PF	With CF
% Voltage Flicker	2.92	2.92	1.78
% Improvement	--	0	39.04

## 5.4 Summary

This chapter describes the simulation and analysis of composite filter for power quality improvement of electric arc furnace distribution network. Distribution network is simulated using Cassie-Mayr and the proposed EAF models. The combined model connected distribution network describes most of the specifications and operational characteristics of EAF. The simulated EAF distribution network is used for power quality analysis-voltage-current harmonics, voltage flicker and voltage unbalance. Next, a control strategy, based on the dual vectorial theory of power, for a composite filter connected in parallel with the unbalance, non-sinusoidal and randomly varying EAF is proposed. Finally, performance of passive filter and series active power filter is compared for various operation cycles of EAFs connected distribution network. Performance comparison shows that, the proposed composite filter performs better than the passive filter alone for harmonic compensation, voltage flicker mitigation, and for clearing voltage unbalance.